

# Rapid growth and catastrophic destruction events of Planchón Volcano, Southern Andes

 José Antonio Naranjo<sup>\*α</sup>,  Jorge E. Romero<sup>β</sup>, Juan Pablo Contreras<sup>α</sup>,  Yuji Orihashi<sup>γ</sup>, Kevin Scott<sup>δ</sup>,  Miguel J. Haller<sup>ε</sup>, and  Hirochika Sumino<sup>ζ</sup>

<sup>α</sup> Departamento de Geología Regional, Servicio Nacional de Geología y Minería, Av. Santa María 0104, Providencia, Santiago, Chile.

<sup>β</sup> Instituto de Ciencias de la Ingeniería, Universidad de O'Higgins. Libertador Bernardo O'Higgins 611, Rancagua, Chile.

<sup>γ</sup> Global Environment and Disaster Prevention Sciences, Graduate School of Science and Technology, Hirosaki University, 1 Bunkyo-cho, Hirosaki, Aomori 036-8561, Japan.

<sup>δ</sup> Cascade Volcano Observatory, United States Geological Survey, Vancouver, Washington, United States.

<sup>ε</sup> Universidad Nacional de la Patagonia San Juan Bosco (UNPSJB). Boulevard Brown 3051. 9120 Puerto - Madryn, Argentina.

<sup>ζ</sup> Research Center for Advanced Science and Technology, The University of Tokyo, 4-6-1 Komaba, Meguro-ku, Tokyo 153-0041, Japan.

## ABSTRACT

During the Late Pleistocene-to-Holocene, the mafic Planchón volcano (35.2 °S, Southern Andes) experienced two important destructive events: a sector collapse to the west and a multiphase explosive eruption transforming the east summit area. We provide new field and laboratory evidence, including geochemical, geochronologic, and geological-morphological analysis, to reconstruct the evolution, triggering mechanisms, and physical parameters of these events. The lateral collapse (48 ka BP) was mainly predisposed by a tectonically westward-inclined substratum and rapid edifice growth rates (0.3–0.48 km<sup>3</sup> ka<sup>-1</sup>). The resulting Planchón-Teno debris avalanche became valley-confined traveling at c. 260 km h<sup>-1</sup> up to 95 km distance and forming an 8.6 ± 1.3 km<sup>3</sup> deposit. The resulting 4.1 km wide amphitheater was later destroyed at c. 7 ka BP by the multiphase Valenzuela phreatomagmatic eruptions, forming a c. 2.5 km diameter caldera. The case of the Planchón volcano warns that rapidly growing mafic volcanoes imply a substantial catastrophic hazard increase for the surrounding areas.

## RESUMEN

El volcán Planchón (35,2 °S, Andes sur) experimentó dos importantes eventos destructivos durante el Pleistoceno Tardío-Holoceno: un colapso sectorial hacia el oeste y una erupción explosiva multifásica que transformó la zona sumital oriental. Aportamos nuevas evidencias de campo y laboratorio (análisis geoquímicos, geocronológicos y geológico-morfológicos) para reconstruir la evolución de estos eventos, sus mecanismos desencadenantes y parámetros físicos. El colapso lateral (~48 ka AP) estuvo condicionado principalmente por un sustrato tectónicamente inclinado hacia el oeste y rápidas tasas de construcción del edificio (0,3–0,48 km<sup>3</sup> ka<sup>-1</sup>). La avalancha de escombros resultante (Planchón-Teno) se confinó en el valle, viajando a unos 260 km h<sup>-1</sup> hasta una distancia de 95 km y formando un depósito de 8.6 ± 1.3 km<sup>3</sup>. El anfiteatro resultante, de 4,1 km de ancho, fue destruido hace ca. 7 ka BP, con las erupciones freatomagmáticas multifásicas de Valenzuela, formando una caldera de ca. 2,5 km de diámetro. Los volcanes máficos de rápido crecimiento, como el Planchón, pueden aumentar sustancialmente el peligro catastrófico para las zonas circundantes.

**KEYWORDS:** Planchon volcano; Volcanic debris avalanche; Paleoglacial environment; Dilute pyroclastic density current; Southern Andean Volcanic Zone.

## 1 INTRODUCTION

Lateral flank failures are catastrophic events that involve the partial destruction of volcanic edifices. They form massive granular flows known as volcanic debris avalanches. The resulting volcanic debris avalanche deposits (VDADs) correspond to massive chaotic breccias with characteristic hummocky morphology composed of detritic material with highly variable grain size (from a few micrometers to decametric blocks). They include consolidated or poorly consolidated fragments of the volcanic edifice, sometimes developing juvenile jigsaw-fit texture, especially when fresh magma is involved [Ui 1983; Glicken 1991; Leyrit 2000; Roverato et al. 2018].

In volcanoes surrounded by irregular topography, the resulting debris avalanches may enter valleys, becoming con-

finied and being longitudinally transformed into debris flows [Scott et al. 2001]. Confined debris avalanches show more extended runout (45–90 km) compared to unconfined examples (<45 km), but also thicker deposits (50–100 m) and elongate flow-parallel hummocks and megaclast-rich lithofacies transported farther down the valley [Keigler et al. 2011]. These characteristics are well represented at Ruapehu volcano (New Zealand), where several volcanic debris avalanches (1.3 to 3.0 km<sup>3</sup>) entrained into deep valleys and gorges (>15 m) producing highly erosive, high shear stress flows that incorporated abundant rip-up clasts of the basement and extend to distances up to 80 km from the source [Tost et al. 2014]. Those much longer runouts up to tens of kilometers dramatically increase volcanic hazard in distal areas [e.g. Scott et al. 2001]. Further transformation of the remnants of collapsed edifices may also occur by destructive events [e.g. Romagnoli et al.

\*✉ jose.naranjo@sernageomin.cl

2009], masking the impacts of the original collapses from the volcano geomorphology.

Planchón volcano (35.2 °S, Southern Andes of Chile, and Argentina; [Figure 1](#)) sourced one of the longest confined debris avalanches of the world, named the Planchón-Teno Debris Avalanche Deposit [PTDAD; [Naranjo et al. 1999](#)]. It corresponds to a monotonous basaltic Pleistocene-Holocene edifice [[Tormey 1989](#); [Tormey et al. 1995](#); [Naranjo et al. 1999](#)] and it lies on the northern part of an ancestral eroded structure, constituted by the Middle-Late Pleistocene Peteroa-Azufre complex ([Figure 2](#)). The PTDAD reached 95 km to the west of the volcano, and its surface is dominated by a hummocky landscape, significantly above terraced landscapes at valley flank embayments, where valley walls did not confine the avalanche, and the depositional fan levées [[MacPhail 1973](#); [Naranjo et al. 1999](#); [Scott et al. 2001](#)]. It is also noteworthy that, despite the preserved volcanic avalanche deposit, the degree of destruction shown by the avalanche caldera that remained after the collapse is unusual ([Figure 3](#)). Indeed, it exhibits a horseshoe-shaped amphitheater open to the south instead of to the west where the avalanche deposit was emplaced [[Naranjo et al. 1999](#)]. Therefore, the Planchón volcano could not only have suffered a single destructive process, but also experienced another catastrophic eruption that modified the initial amphitheater. This event would be represented by the deposition of the diluted and concentrated Valenzuela Pyroclastic Density Currents (VPDC) during the Holocene [[Naranjo et al. 1999](#); [Naranjo and Haller 2002](#)].

There is controversy on the evolution of Planchón volcano and the timing of the different events that have affected its structure (see [Table 1](#) for comparisons). In fact, [Tormey \[1989\]](#) and [Tormey et al. \[1995\]](#) mentioned that the debris avalanche excavating the summit amphitheater may have been accompanied by a biotite-rhyodacite pumice eruption. However, [Naranjo et al. \[1999\]](#) and [Naranjo and Haller \[2002\]](#) showed that the only rhyodacite pumice eruption occurred much later than the Upper Pleistocene Planchón amphitheater formation, when the Los Ciegos PDC eruption took place toward the eastern flank during the Common Era (CE) at  $1.400 \pm 80$  and  $1.050 \pm 90$  BP. These authors also demonstrated that Azufre Volcano forms the northern part of the Peteroa-Azufre complex and was cut by the collapse and formation of the amphitheater and not by the explosive volcanic activity of the previously extinct Peteroa volcano.

This work seeks to: 1. Update and reinterpret the volcano-stratigraphy of Planchón volcano, considering paleo-environmental conditions and the modifications of the volcanic morphology along its evolution; 2. Explain the architecture, triggering mechanisms, and the physical parameters leading to the PTDAD and VPDC deposits west and east of Planchón volcano, respectively; 3. Explore the apparent geochemical homogeneity of Planchón products along its evolution, and 4. Propose hazard considerations for similar volcanic systems.

## 2 GEOLOGICAL BACKGROUND

### 2.1 Geological and structural setting

Basement rocks in the area include NNE-trending belts of folded and thrust marine sedimentary sequences and volcanic rocks of Upper Jurassic to Cretaceous age to the east, and sedimentary, volcanic, and volcanoclastic rocks intruded by granodioritic stocks with Cenozoic age to the west [[Davidson and Vicente 1973](#); [Charrier et al. 1994](#); [Flynn et al. 1995](#); [Naranjo et al. 1999](#); [Charrier et al. 2002](#); [Fock et al. 2006](#); [Piquer et al. 2010](#); [Rossel et al. 2014](#); [Mosolf et al. 2019](#)]. According to these authors, from older to younger, these sedimentary rocks are: 1) sandstones, conglomerates, and fossiliferous limestones of the Baños del Flaco Formation (Upper Jurassic); 2) sandstones and red conglomerates with interbedded volcanic rocks of the Río Damas Formation (Late Jurassic-Early Cretaceous); 3) Lower Cretaceous sedimentary and volcanic rocks of the Colimapu Formation, lying in contact by thrust faulting with the Jurassic units; 4) Cenozoic volcanic, volcanoclastic, and pyroclastic rocks of the Abanico Formation (Late Cretaceous to Miocene), mainly outcropping to the northwest of the volcano. These younger rocks have been intruded by Miocene-Pliocene granodioritic, tonalitic, and dioritic stocks and dikes [[Piquer et al. 2010](#)].

The tectonic structures associated with the PPVC are the El Fierro fault system (EFFS) and Infiernillo-Los Cipreses faults (ILCF; [Figure 1](#)). The EFFS is a NNE–SSW reverse fault dipping 45–50° to the west [[Davidson and Vicente 1973](#); [Piquer et al. 2010](#); [Vigide et al. 2020](#)]. It corresponds to the southernmost segment of a regional-scale structure named El Diablo-Las Leñas-El Fierro fault [e.g. [Charrier et al. 2002](#); [Fock et al. 2006](#); [Farías et al. 2010](#); [Charrier et al. 2019](#)]. The EFFS has a reverse kinematic, and its hanging wall is represented by the Late Cretaceous to Miocene Abanico Formation, while the footwall corresponds to the Late Upper Jurassic Baños el Flaco and Late Jurassic-Early Cretaceous Río Damas formations. On the other hand, ILCF corresponds to several minor reverse faults located west of EFFS, developing NE–SW and N–S trending structures dipping 65–70° W. Quaternary-to-recent strike-slip regime, with an ~ENE–WSW trending  $\sigma_1$ , and a sub-vertical  $\sigma_2$ , has been suggested to favor hydrothermal fluid circulation in the intersections of these main faults with transverse ~NE–SW and ~WNW–ESE structures [[Vigide et al. 2020](#)]. However, following the same geomorphologic pattern along tributary valleys, we infer a remarkably more complex structural network (including lineaments) for fluid circulation composed of a more significant number of both main N–S trending and oblique (conjugate) structures, as shown in [Figure 1](#).

### 2.2 Geology of the Planchón volcano

The evolution of the Planchón-Peteroa Volcanic Complex (PPVC) has been constrained by the works of [Tormey \[1989\]](#) and [Tormey et al. \[1995\]](#), [Haller et al. \[1991, 1994\]](#), [Naranjo et al. \[1997, 1999\]](#) and [Naranjo and Haller \[2002\]](#), who have described several evolutionary stages. A summary of their constraints and descriptions is presented in [Table 1](#). Planchón volcano (35.2 °S, 70.6 °W, 3977 m asl) corresponds to the

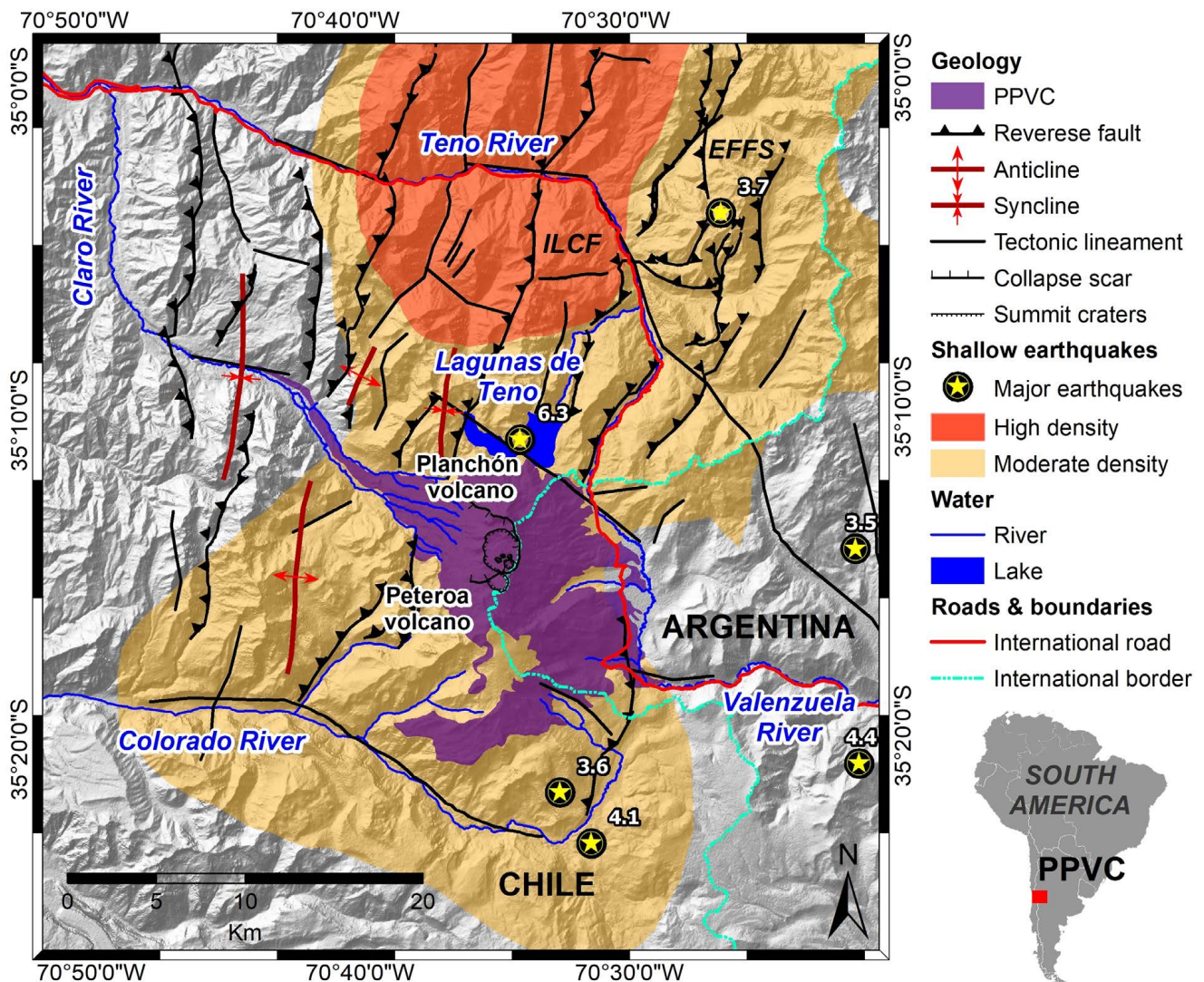


Figure 1: Location map of Planchón-Peteroa Volcanic Complex (PPVC) and its tectonic features [after Davidson and Vicente 1973; Piquer et al. 2010]. Significant earthquakes ( $M > 3$ ) [Vigide et al. 2020] are represented by stars. High (5.6 events/10 km<sup>2</sup>) and moderate (0.4 events/10 km<sup>2</sup>) earthquake density based on the NEIC (USGS) shallow tectonic seismicity (<10 km depth) database between 1985 and 2021. The uncolored areas have a low earthquake density of <0.4 events/10 km<sup>2</sup>. Main faults systems are indicated (El Fierro fault system (EFFS) and Infernillo-Los Cipreses faults (ILCF)). Digital elevation model (DEM) from ALOS-Palsar mission, with 12.5 m spatial resolution.

northern limit of the Planchón-Peteroa-Azufre volcanic complex (PPAVC). Peteroa-Azufre is a deeply eroded Upper Pleistocene volcanic edifice with two new <sup>40</sup>Ar/<sup>39</sup>Ar ages of  $219 \pm 14$  and  $178 \pm 5$  ka (Figure 2), thus suggesting its activity to have occurred between ~300 and 150 ka [Klug et al. 2022]. The volcano was previously known as Azufre [e.g. Davidson and Vicente 1973; Haller et al. 1991; 1994; González Ferrán 1995] and is mainly composed of alternating lava flows and pyroclastic deposits with basaltic, basaltic andesite, andesitic, and dacitic composition reaching up to 68 km<sup>3</sup> [Tormey 1989; Tormey et al. 1995; Naranjo et al. 1999; Naranjo and Haller 2002].

According to the most up-to-date works [Naranjo et al. 1999; Naranjo and Haller 2002], the first edifice (Planchón 1) grew up through a dominant basaltic and basaltic andesite effusive

eruptive style during the Upper Pleistocene, reaching a volume of 25–30 km<sup>3</sup>. The maximum age of Planchón volcano is given by maximum and minimum plateau ages of c.  $191 \pm 6$  and  $153 \pm 3$  ka of the Peteroa-Azufre complex [Klug et al. 2022]. In addition, new <sup>40</sup>Ar/<sup>39</sup>Ar dating yield plateau ages of  $49 \pm 17$  and  $49 \pm 14$  ka for the main edifice of Planchón volcano and  $21 \pm 10$  ka [Klug et al. 2022] for an eruptive center located 4 NE of the summit that we denominate here as Domo Teno volcano (Figure 2).

Previously, the Planchón edifice experienced a catastrophic lateral collapse during the Upper Pleistocene producing extensive PTAD, reaching c. 10 km<sup>3</sup> and a runout distance of 95 km to the west [Naranjo et al. 1997; 1999; Scott et al. 2001; Naranjo and Haller 2002]. The chaotic debris avalanche was channelized along the Claro and Teno glacial valleys, extend-

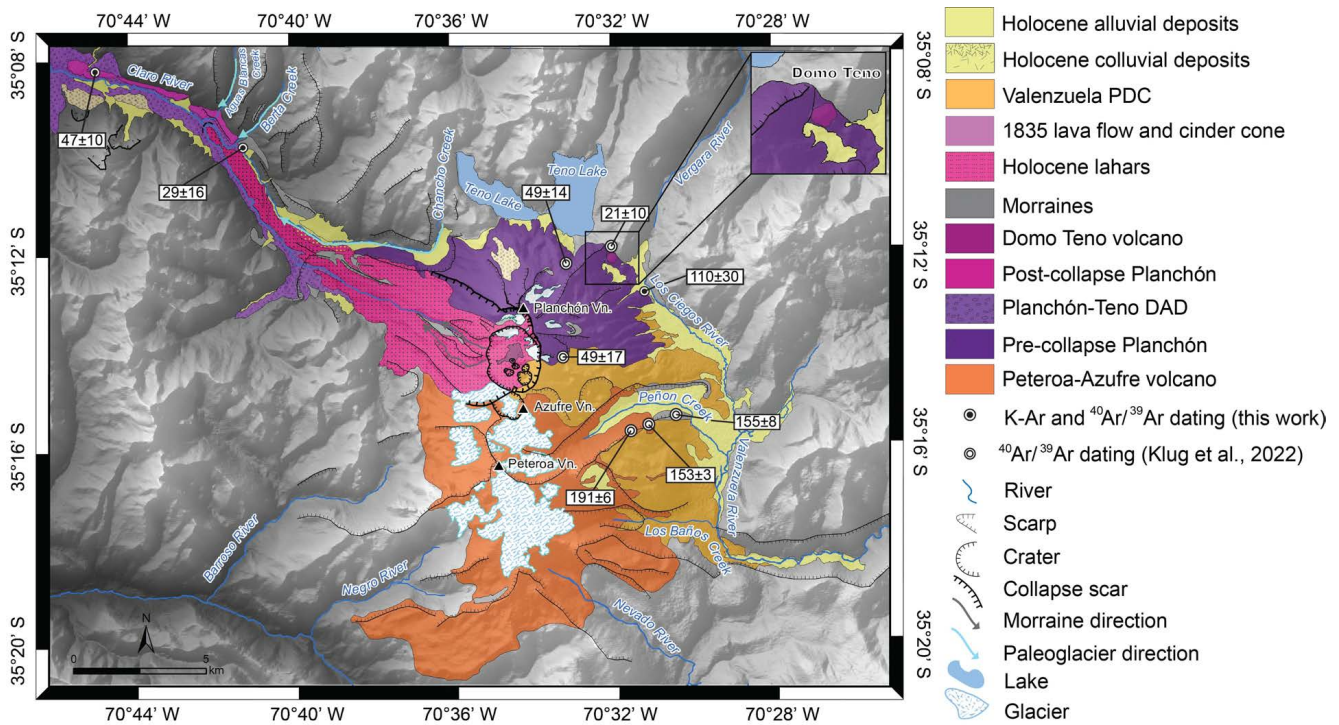


Figure 2: Updated geologic map of the Planchón-Peteroa volcanic complex. Ages are given in ka. The digital elevation model (DEM) was acquired from the ALOS-Palsar mission, with 12.5 m spatial resolution.

ing northwest to the Coastal Cordillera (Figure 4). In these valleys, the PTDAD locally covers c. 370 km<sup>2</sup> of fluvioglacial deposits.

Subsequently, Planchón continued erupting basaltic lavas during the Upper Pleistocene, configuring the 3.5 km<sup>3</sup> post-collapse edifice [Naranjo et al. 1999; Naranjo 2012]; its lavas extended to the west down the Claro River glacial valley (Figure 2). The avalanche is locally covered by these lavas (<23 km from the source), as well as by local Quaternary landslide deposits and alluvial fans [Naranjo et al. 1999].

Considering the eruptive style, Planchón volcano developed particularly effusively as a simple volcanic structure whose sector collapsed to the west, and the pyroclastic surge of the Holocene VPDC to the east only represented scattered interruptions in its monotonous growth through a dominantly effusive style.

The most recent activity of Planchón is evidenced during the Early Holocene (c. 7 ka) by a series of subglacial phreatomagmatic explosive eruptions which formed nearly 0.08 km<sup>3</sup> of pyroclastic density current (PDC) and tephra fall-out deposits with andesitic composition, affecting the eastern side of the volcano [Naranjo and Haller 2002]. These eruptions were also accompanied by the formation of lahars to the west. Further, a sub-Plinian tephra fall eruption (Los Baños Pumice) occurred at 1.0–1.5 ka and erupted mingled dacitic/andesitic pumice. During historical times (i.e. <400 years), low volcanic explosivity eruptions (VEI 1–2) have occurred. Most corresponded to weak phreatic and phreatomagmatic events as observed since the 1991 CE eruption [Naranjo et al. 1999; Carrasco 2002; Naranjo and Haller 2002; Naranjo 2012; Aguilera et al. 2016; Romero et al. 2021]. From these eruptions, Naranjo

[2012] suggested that the only one that evidenced purely effusive origin during the Holocene occurred in 1837 CE, two years after the 1835 CE megathrust earthquake that affected central Chile. Furthermore, the February 27, 2010 Mw 8.8 Maule earthquake (same rupture zone as in 1835 CE) disrupted the shallow magmatic-hydrothermal system releasing magmatic fluids from two shallow crystallizing intrusions [Haller and Risso 2011; Naranjo 2012; Aguilera et al. 2016]. According to Bonali et al. [2013], the 2010 earthquake decreased normal stress on the feeding system (unclamping) of Planchón Peteroa, promoting dyke intrusion and volcano awakening, however no juvenile material was erupted. Contrarily, in 2018/19 a trachyandesite magma fed the phreatomagmatic eruptions of PPAVC [Romero et al. 2020].

### 3 METHODS

#### 3.1 Field mapping

Early mapping and former deposit descriptions were carried out by Davidson and Vicente [1973], followed by Tormey [1989], Tormey et al. [1995] and Haller et al. [1991, 1994]. Later, the geologic units were redefined and reinterpreted by Naranjo et al. [1999], also releasing the hazard maps of the PPVC. Accessing the volcano’s west flank was only possible by helicopter because of the scarce roads in the area. Oblique aerial views allowed the recognition and inspection of deep gorges where the Claro River dissects the VDAD. Further visits complemented observations during ascents to both western and eastern volcano flanks during the southern hemisphere summers of 2006, 2010, and 2011. Later observations on the PTDAD were carried out in mid-2021 (Table 2). When a di-

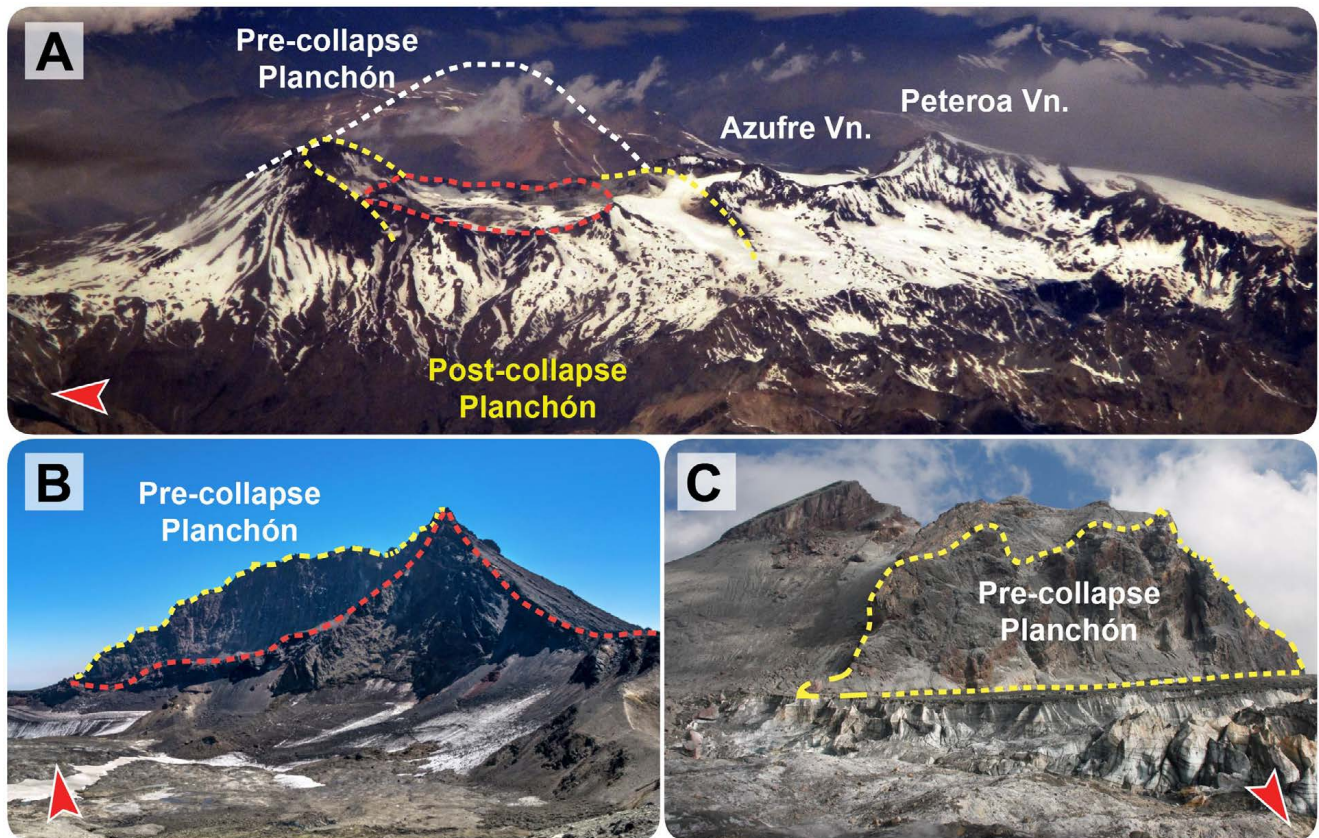


Figure 3: Morphology of the Planchón-Peteroa volcanic complex. [A] Aerial view to the east of the Planchón-Peteroa volcanic complex showing the likely pre-collapse cone (white dotted line), the remnants of the sector collapse scar (yellow dotted line), and the caldera of the post-7 ka BP multiphase Valenzuela eruption of Planchón volcano (red dotted line). [B] Viewing north, cross-section photograph of the pre-collapse Planchón edifice and the post-collapse Planchón caldera. [C] Viewing south, internal remnants of the pre-collapse Planchón edifice. Photos B and C by Esteban Berrío. The red arrow points to the north.

rect inspection of field outcrops was possible, stratigraphic and sedimentologic observations were performed. Occasionally, lava samples from Planchón Volcano and post-collapse lavas were collected for unspiked K-Ar and Ar/Ar dating and geochemical analysis (see details below). In summary, during the field work, a total of approximately 250 locations were checked, in which descriptions, measurements, and selective sampling were carried out.

Field and aerial observations were complemented by using Google Earth™ imagery and ALOS-Palsar digital elevation models (12.5 m resolution). These first were also used for the recognition and measurement of the largest-size hummocks, and according to Potere [2008] and Sharma and Gupta [2014] the horizontal and vertical accuracy have root-mean-squared errors (RMSE) of 39.7 m and  $1.355 \pm 0.5284$  m, respectively. Regarding the volume of the debris avalanche deposit, it was subdivided in 10 irregular polygons representing known average thicknesses observed in the field. Polygon areas were measured using Google Earth™ and then multiplied by their respective thicknesses. In some sections, we expect an error as large as 15 % due to the underlying geometry of the valley infill. We quantified each hummock's height, length, width, area, and distance from the vent. The heights were constrained by direct observation. Statistical analyses

of the information retrieved from these measurements allow us to determine the main elongation direction of these hummocks and their morphometric relationships with distance from the source, thus providing valuable information to infer flow kinematics and emplacement dynamics [e.g. Yoshida 2013; Paguican et al. 2014].

### 3.2 Sample preparation, lithological and textural analyses

In addition to the previous sampling available by Naranjo et al. [1999], we collected ten lava samples for geochemistry and K-Ar and Ar/Ar dating and three bulk matrix samples from the PTADAD deposit for further grain size analysis. The choice of sampling sites and target units was intended to complement the previous works and constrain the ages and compositions of the pre- and post-collapse Planchón and the PTADAD. Samples for K-Ar and Ar/Ar dating were selected based on mesoscopic and microscopic observations. The samples were crushed into roughly less than 5 mm fragments by a jaw crusher and sieved to 60 to 80 mesh size. The grains were cleaned with ion-exchanged water using an ultrasonic cleaner for about 15–30 minutes after being rinsed several times with distilled water. The ferromagnetic minerals were separated using a hand-magnet. As for K-Ar dating, the same material was used for both K concentration and Ar isotope analyses.

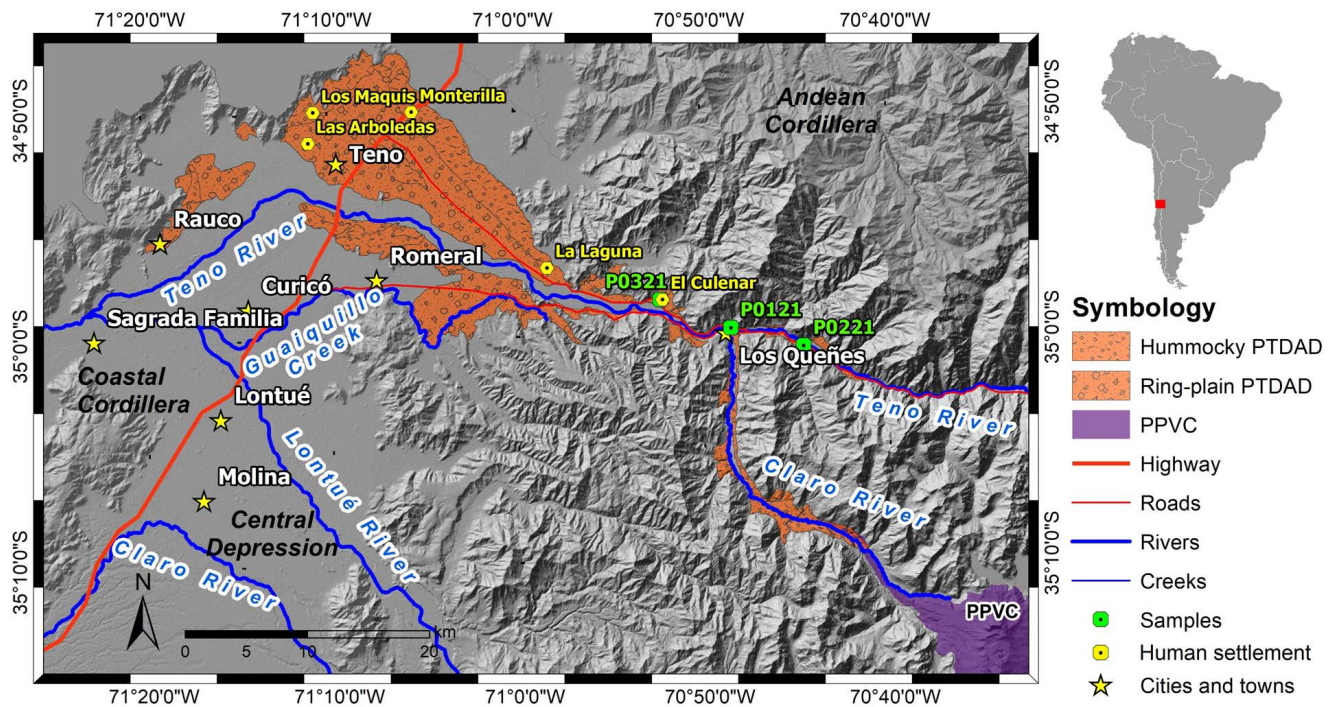


Figure 4: Distribution of the 48 ka Planchón-Teno debris avalanche deposit (PTDAD) modified from Naranjo et al. [1999]. The sampling sites of Figure 6 are shown in green, and the locations shown in yellow correspond to those of Figure 7.

Grain size analyses on bulk sediment matrix samples were carried out by handshaking using a sieve column composed of 7 meshes ranging from 1000 to <75 microns. The 1000-, 500-, and 250-micron fractions were separated for further analysis. The first was only described by hand separation of the different lithologies, while the second was inspected under a binocular microscope and the latter in a scanning electron microscope. These particles were carbon-coated and analyzed with the FEI Quanta 650 FEG-SEM electron microscope (Department of Earth and Environmental Sciences, University of Manchester) operated at 10 kV, beam current of 10 nA, and a working distance of 10 mm. We collected backscattered and secondary electron images (BSE and SE, respectively).

### 3.3 Geochronology and geochemistry

This study employed the unspiked technique for K-Ar dating because this method can precisely date rocks younger than 0.1 Ma [e.g. Gillot et al. 1982; Nagao et al. 1991; Orihashi et al. 2004; Guillou et al. 2010; Grosse et al. 2018]. Ar analyses were performed using a noble gas mass spectrometer MS-III (modified-VG5400) in the Laboratory for Earthquake Chemistry, Graduate School of Science, University of Tokyo. K concentration was determined by the X-ray fluorescence (XRF) (Phillips PW 2400) at the Earthquake Research Institute, the University of Tokyo. More details on the method, standard and uncertainty calculation were described in Nagao et al. [1991] and Orihashi et al. [2004]. The results are shown in Table 3. The obtained  $^{38}\text{Ar}/^{36}\text{Ar}$  ratio was  $0.18814 \pm 0.0049$  ( $1\sigma$ ), which is in agreement with the modern atmospheric value of 0.1880 within the range of analytical error. This indicates that

there was none of the air fractionation effect for the sample (NPP-33).

Ar/Ar dating was carried out at the Laboratorio de Geocronología at the Servicio Nacional de Geología y Minería (SERNAGEOMIN, Chile). Samples were pulverized and separated using a Frantz Isodynamic Magnetic Separator, while ground mass was selected using a binocular microscope. The sample was irradiated with fast neutrons for 24 hours at the Chilean Nuclear Energy Commission. For the cooled sample,  $^{40}\text{Ar}/^{39}\text{Ar}$  stepwise heating analyses were achieved at the Geochronology of the SERNAGEOMIN, Chile using a Frantz Isodynamic Magnetic Separator. “Fish Canyon” tuff ( $28.03 \pm 0.10$  Ma [Renne et al. 1994]) was used to monitor for the neutron flux in this study. Based on  $^{40}\text{Ar}/^{39}\text{Ar}$  plateau defined by Fleck et al. [1977],  $^{40}\text{Ar}/^{39}\text{Ar}$  plateau age was calculated. More detailed procedures were described in Pérez de Arce et al. [2003].

Chemical analyses were carried out at the Earthquake Research Institute, the University of Tokyo. Rock samples were crushed and pulverized to less than 60  $\mu\text{m}$  diameter, then mixed in a 1:3 ratio with a mixture of lithium metaborate and lithium tetraborate, where the final ratio of sample and this mixture is 1:2. Major element and some trace element (Sc, V, Cr, Co, Ni, Zn, Ga, Rb, Sr, Y, Zr, Nb, Ba) compositions were determined by XRF (Phillips PW 2400), where they were fused into a glass bead. Using the same glass bead, the other trace element (REE, Hf, Ta, Pb, Th, U) compositions were determined by laser ablation-ICP-MS (VG PQ3 combined with New Wave UP-213). More details on both methods were described in Tani et al. [2002] and Orihashi and Hirata [2003], respectively. Rare Earth Elements (REE) geochemistry was

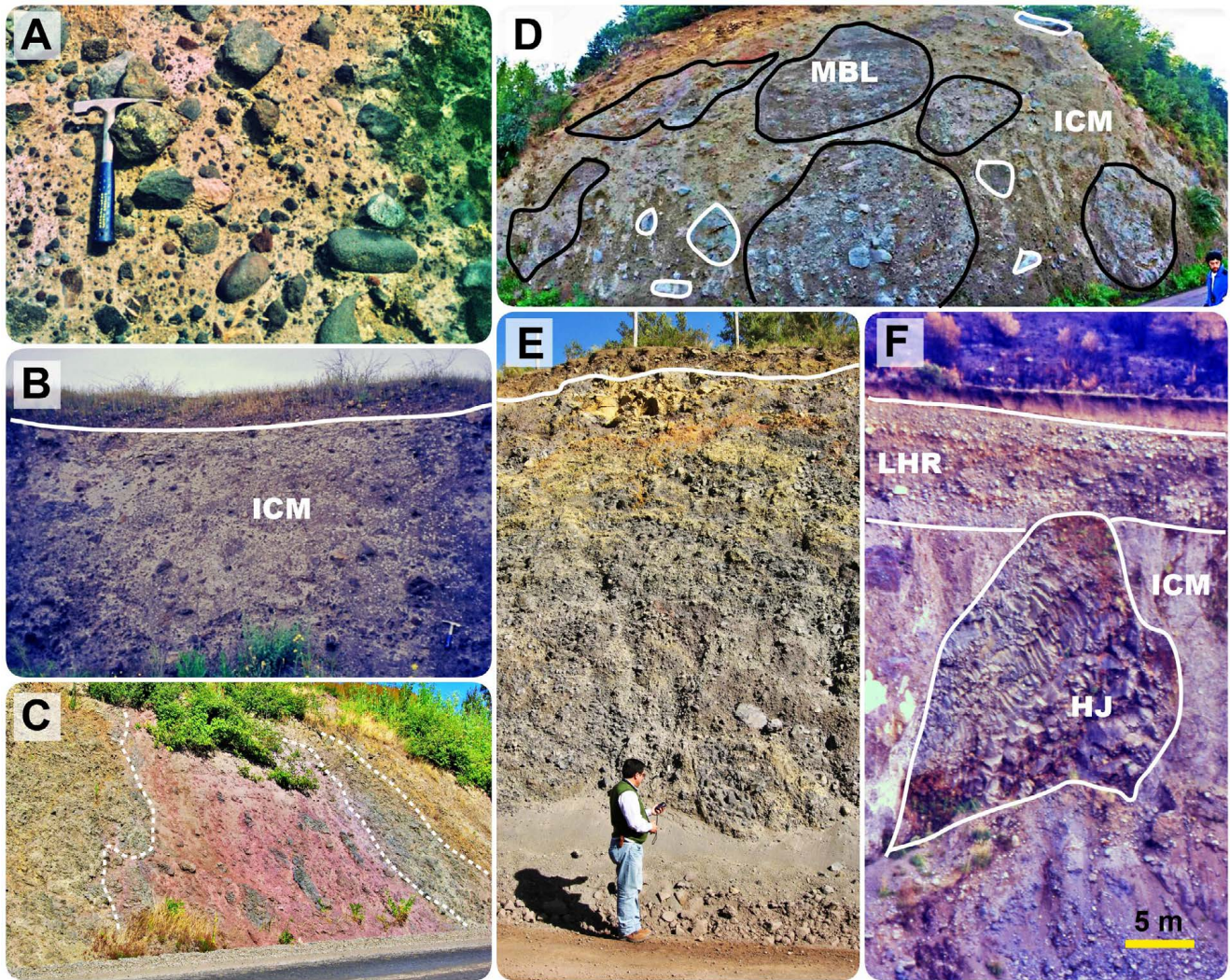


Figure 5: Facies of the Planchón-Teno debris avalanche deposit (PTDAD). [A] Matrix facies found near Teno, ca. 70 km distance from the source. These facies contain abundant subrounded clasts incorporated from the fluvial bed during the emplacement of the DAD. [B] Matrix facies at a railroad exposure, ca. 68 km NW from the source. The intraclast matrix (ICM) is fine-grained and indurated. [C] Mixed facies at El Culenar, 40 km NW from the source. The white segmented lines show the contacts between different lithological domains. [D] Mixed facies in a roadcut near Romeral, ca. 34 km NW from the source. The indurated ICM supports mega blocks (MBL) and clasts (white polygons). [E] Highly triturated edifice block facies near Estero La Jaula, ca. 29 km NW from the source, mainly composed of gray basaltic and basaltic andesite fragments. [F] Fluvial terrace of the Claro River ca. 13 km WNW from the source, which exposes the mixed facies of the DAD and a giant, ca. 20 m-long hackly-jointed basaltic lava. Lahar (LHR) deposits overlaid the avalanche deposit in erosive contact.

normalized to chondritic values, and spidergrams from the obtained data were normalized to the primitive mantle [Sun and McDonough 1989].

## 4 THE PLEISTOCENE SECTOR COLLAPSE

### 4.1 Collapse amphitheater

The original shape delimiting the escarpment formed after the Planchón sector collapse (avalanche caldera) has been masked, exhibiting an irregular expression. According to Tormey et al. [1995], the remnants of the edifice were dissected by glaciers and explosive activity preserved as proximal pyroclastic deposits, and covered by radially dipping lavas of basaltic to basaltic andesite composition. The escarpment is

more evident in the northern part (Figure 3A), with a maximum avalanche scar height of 3935 m asl, which exhibits a horseshoe-shaped opening (amphitheater) of c. 1.5 km across, but open to the south. On the eastern edge, however, it shows a saddle segment at about 455 m lower (3480 m asl) than the northern scarp (Figure 3B). To the SW, the discontinuous collapse scarp reaches a height of 3655 m asl at the expense of the ancient Azufre Volcano (Figure 3C). Down the Río Claro to the WNW, only the northern escarpment can be seen as the southern one was obliterated by glacial erosion.

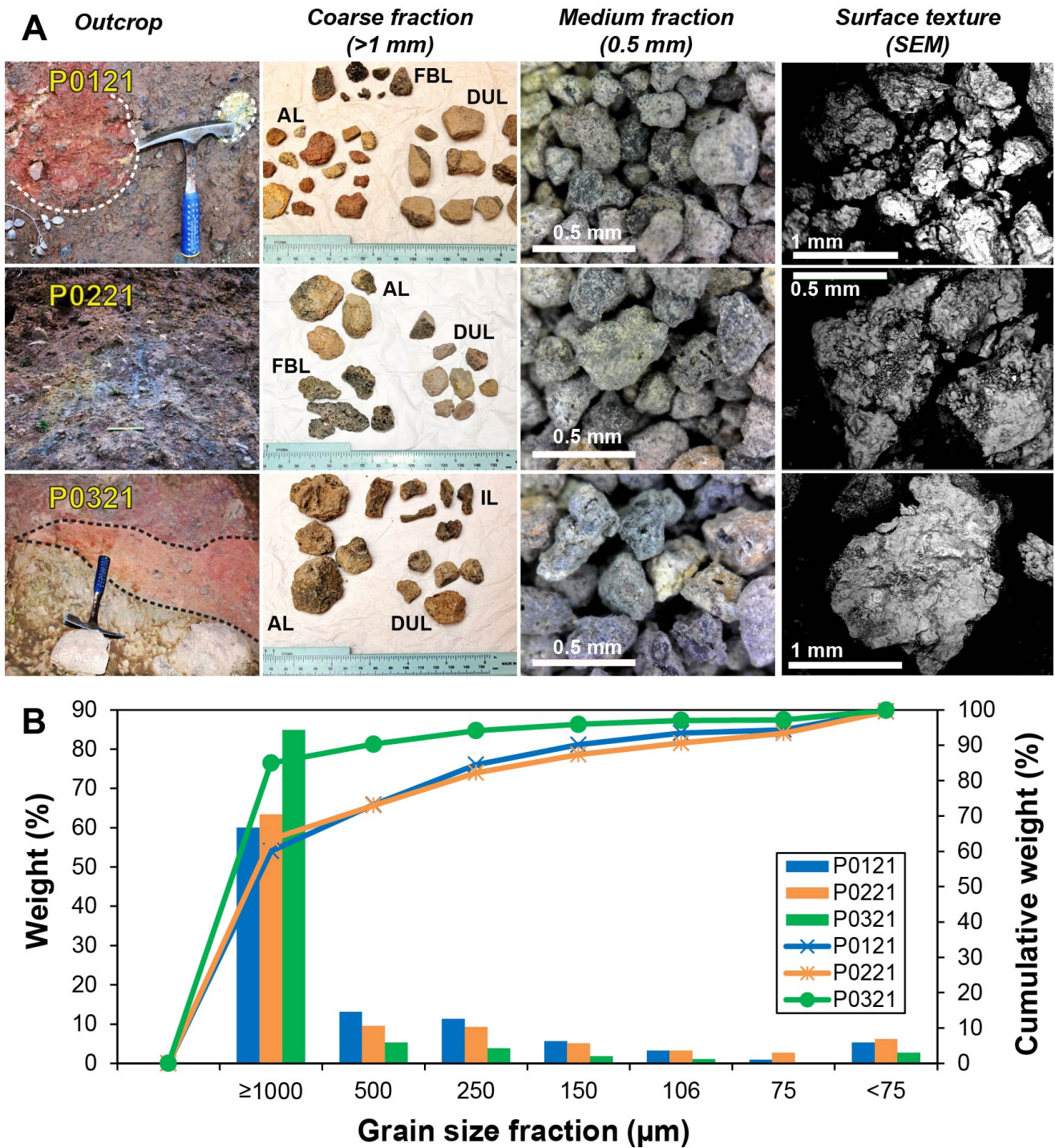


Figure 6: Sedimentology of the PTAD matrix. [A] Textural and compositional characteristics of the matrix constituents by grain size fraction. AL= altered (oxidized) lithics, DUL=Dense unaltered lithics, FBL= Fresh (unaltered) blocky lithics, and IL=Irregular-shaped lithics. Most of the particles in the medium fraction are subangular to subrounded and contain none to low vesicularity. The scanning electron microscope (SEM) images show highly triturated particles with irregular surfaces, jigsaw-fit cracks, and staircase surfaces in subangular larger (mm-sized) particles. [B] Grain size distribution of three samples indicated in [A]. These samples are: P0121= Romeral, P0221=Estero La Jaula, and P0321=El Culenar.

4.2 Planchón-Teno debris avalanche deposit (PTDAD)

Although the PTDAD has been described at distal hummocky outcrops in MacPhail [1973], it was initially classified as a lahar. Further work carried out by Davidson and Vicente [1973]

and Tormey [1989] provided general descriptions on the geometry of the deposit, that was later dated by Hauser [1990, 1993] in 12 ka using <sup>14</sup>C. However, Naranjo et al. [1997, 1999], who describe in more detail the geometry, mobility, and some

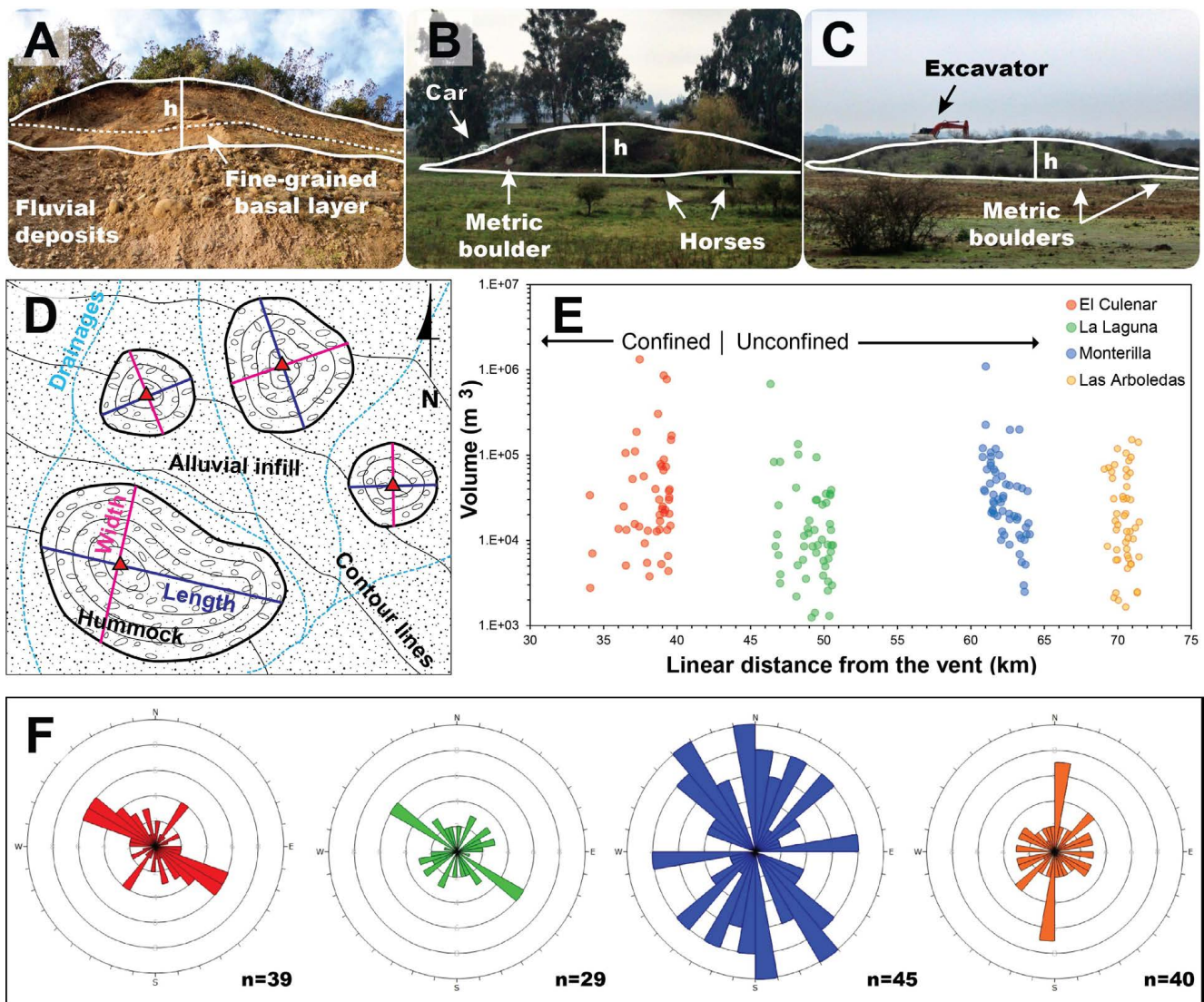


Figure 7: Morphology, geometry, and elongation of the PTAD hummocks. [A] Longitudinal exposure of a hummock at El Culenar, overlying fluvial deposits. The dashed line indicates the boundary between the lowermost fine-grained (matrix-rich) layer and the upper mixed facies. [B] and [C] show hummocks at Monterilla and Los Maquis (64 and 70 km NW from the source), respectively. [D] Cartoon on the geometric measurement of hummocks (red triangle=height above the surrounding land). Heights are available in [Supplementary Material 1](#). [E] Variation of the hummock volume with linear distance NW from the source. [F] Rose diagrams showing the central elongation axis of hummocks (see E for color key). Numbers represent the size of the sample.

internal features of the deposit, disagreed with the age as they observed glacially eroded lavas on top the avalanche deposit. Later, [Scott et al. \[2001\]](#) added brief descriptions of distal facies and grain size characteristics of the matrix. Our work provides new observations on the distribution, proximal-to-distal facies analysis, a morphometric characterization of hummocks, grain size and componentry analyses, velocity estimates, a revised volume, and a geochronologic framework for the PTAD.

The PTAD proximal outcrops display maximum exposed thicknesses between 30 and 50 m. From the confluence of Claro and Teno rivers at Los Queñes ([Figure 4](#)), the deposit is found 13 km upstream of the Teno River valley, reaching up to an altitude of 950 m asl which means a topographic run-up of 270 m to the east. In the Central Valley, to the west, the deposit is c. 25 m thick and forms a 16 km-wide and 28 km-long debris

fan, which extends to the town of Teno and the lower slopes of the Coastal Cordillera near Rauco, 175 m asl ([Figure 4](#)). The fan margins developed 5–10 m-high lateral levées with 2–3 km width and a main central channel of 9 to 10 km width. A revised volume considering an average thickness of c. 23 m yields a more accurate estimation of  $8.6 \pm 1.3 \text{ km}^3$  Planchón-Teno debris avalanche deposit (PTDAD).

A detailed description of the deposit facies is available in [Table 2](#). In the distal fan, the deposits constrained between the levées develop an upper bed of less consolidated, occasionally loose material with thicknesses up to 3 m. The central deposit is matrix-supported, and the matrix has brown-pink color containing rounded accidental clasts of gravel up to 1 m in size (>20 %) with bimodal texture ([Figure 5A, B](#)). On the contrary, the medial sites near El Culenar con-

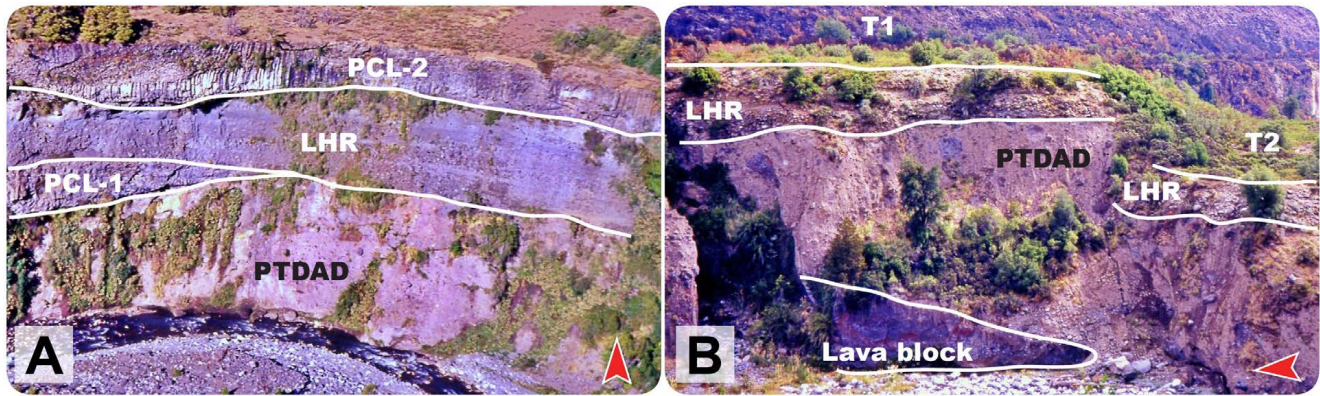


Figure 8: Post-collapse lavas (PCL) and lahar (LHR) deposits exposed in gullies along the Claro River (ca. 14 km west from the source). [A] The lahars are interbedded between them. [B] The erosion of the PTAD is evidenced by terraced (T1 and T2) lahars. Giant lavas lava blocks are observed at the bottom. The red arrow points to the north.

tain fractured clasts and blocks and are incorporated into a multicolor matrix probably resembling the original lithologies that were fragmented (Figures 4, 5C). Near Romeral, the medial deposit consists of a chaotic assemblage of highly triturated, grey basaltic blocks together with less cohesive reddish blocks (Figures 4, 5D). Subrounded intrusive accidental basement rocks are also frequent in most of the grain size fractions. The medial outcrops also include highly triturated block facies containing monolithologic domains, mainly composed of basaltic and basaltic andesite porphyritic fragments that did not disaggregate completely (Figure 5E). In addition to the different degrees of fragmentation, ductile deformation leading to a wavy fashion of the original block's stratigraphy is noticed. The most proximal facies are characterized by a homogeneous texture, with coarse fragments reaching decametric size, represented by hackly-jointing basalt megaclasts and other minor clasts and blocks. They are all included in a finer-grained interclast matrix with particles sizing between sand and coarse gravel (Figure 5F).

The interclast deposit matrix has a grey to gray-purple and reddish color because of fresh, plagioclase, and porphyritic olivine basalts and basaltic andesite fragments with identical texture to those of Planchón 1 (Figure 6A). The interclast matrix is locally compact and well consolidated. It is composed of fine-grained subangular fresh and oxidized lithics, subrounded to subangular basaltic scoria lithics, subangular dense unaltered lithic fragments, irregular lithics (Figure 6A) and free crystals of plagioclase and olivine. Irrespective of the location and color, between 60 and 80 % of the matrix weight is >1 mm, and <10 % is smaller than 75 microns (Figure 6B).

One of the most characteristic morphologic features of the PTAD is the hummocky surface (Figure 7). The hummocks are mainly located in the lateral banks (levées) of the distal fan, the front of the avalanche where it collided with the Coastal Cordillera, and lately in the northern bank of Teno River near Culenar, 6 km west of Los Queñes (Figures 4, 7A–C). Hummocks show lengths between 24 and 323 m and widths from 8 to 173 m (Figure 7D). Only 11 % of hummocks are below the RMSE of the images used for horizontal measurements, while 23 % fall below the vertical RMSE; in consequence, most of

the data is sufficiently accurate and errors should not be larger than one order of magnitude. Their length–width ratio varies from 0.93 to 5.10, with an average of 1.50. Volumes are highly variable, from c. 1200 to 1.3 m<sup>3</sup>, but the overall tendency is to decrease with increasing distance from the source (Figure 7E). While closer to the source, the hummocks are elongated with a northwest orientation (like that of the valleys draining from the volcano) in distal areas (i.e. at the Central Depression) their orientations are chaotic. On the other hand, the hummocks at the front of the avalanche deposit are almost orientated N–S (Figure 7F).

#### 4.3 Post-collapse lahar sequence

In multiple outcrops, the avalanche deposit is covered by up to c. 15 m thick alluvial deposits, with diffuse bedding formed of grey to purple, coarse-grained breccias composed of subangular clasts (Table 2).

At an elevation of 1400 m asl at the Planchón River—10 km WNW of the volcano—a remarkable succession of ancestral lahar deposits is observed, with a total thickness close to 30 m and composed of about five individual deposits, 3–6 m thick, flow units (Figure 8A). The slope of the deposits reaches 0.15 m/m (–8.5°). They commonly include angular blocks up to 2 m in diameter. The post-collapse lavas that form the terraces in the upper Claro Valley, c. 13 km downstream from the volcano, show glacial striations on their top and are also covered by subrounded to subangular, poorly sorted reversely graded alluvial beds composed of imbricated basaltic cobbles and pebbles within a sandy matrix (c. 25 %). These deposits are not part of the glacial till that forms lateral and central moraines, which also contain metric-sized erratic blocks on the surface. More than 15 km downstream, lahar deposits cover at least two terraces in the Claro Valley, carved out of the PTAD (Figure 8B).

According to Naranjo et al. [1999] and Naranjo and Haller [2002], the most extensive lahar deposits would have originated due to the post-collapse Planchón lava effusion, which due to their high emission rate, would have been capable of melting vast masses of a glacier cap much larger than today. Thus, high-energy lahars were generated by removing large

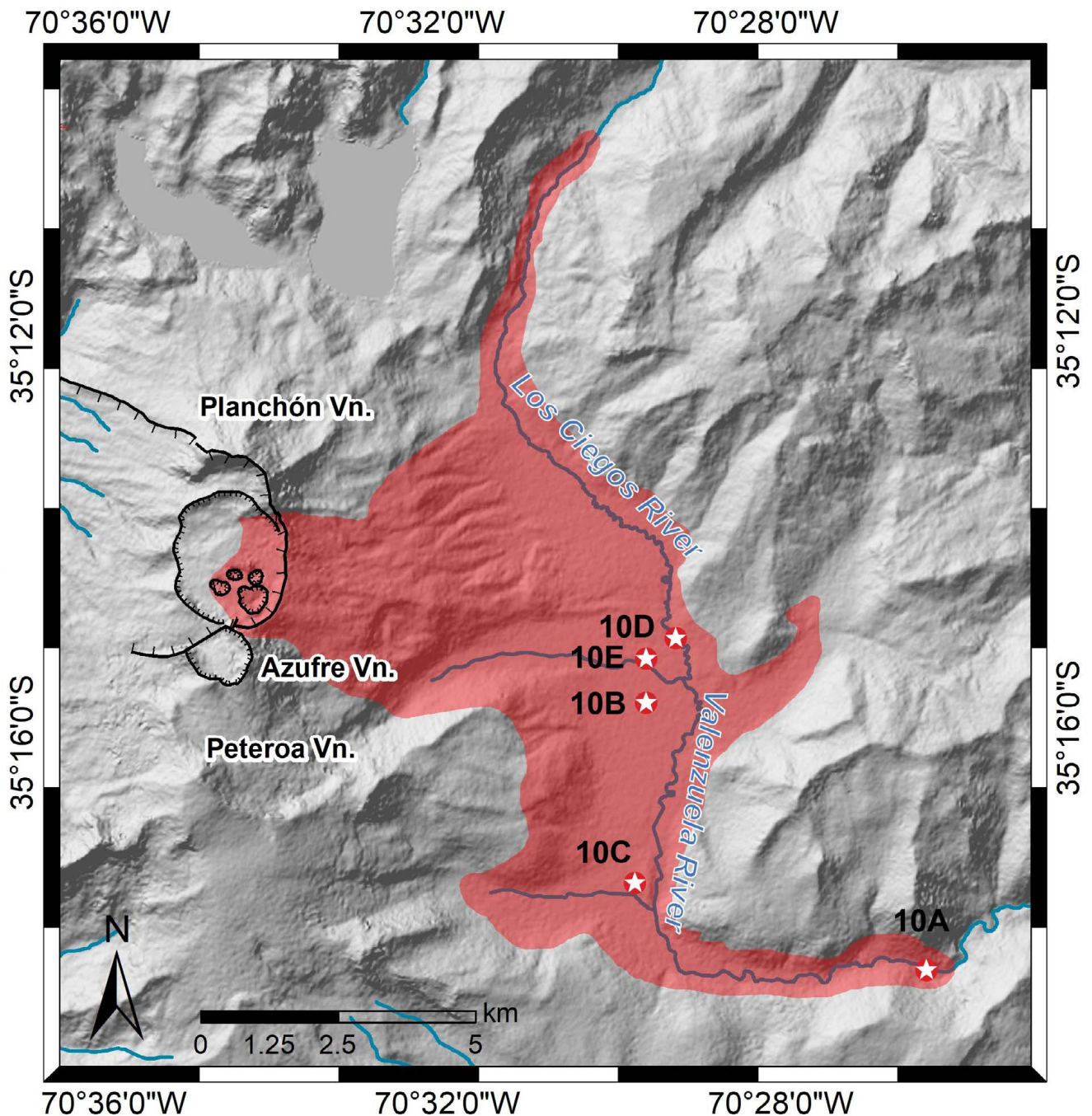


Figure 9: Distribution of the 7 ka Valenzuela Pyroclastic Density Current deposit (VPDC) modified from [Naranjo and Haller \[2002\]](#). Stars represent the location of stratigraphic sections shown in [Figure 10](#).

volumes of available moraines. Other proximal lahar deposits recognized towards the northeast of Planchón by [Tormey \[1989\]](#) are not correlated to this sequence as being glacially eroded and containing pillow basaltic lavas, thus probably indicating a much older, initial phase of volcanic activity.

#### 4.4 PTAD age

Although it is difficult to determine the age of the collapse, it is possible to indirectly constrain the date of the catastrophic event. Presently, the best limit to the minimum age is provided by the presence of glacial forms and deposits above the

PTDAD, as well as basaltic lava flows dated in  $46.5 \pm 10.4$  ka and  $29 \pm 16$  ka (see [Table 3](#) for details). On the other hand, the maximum PTAD should be constrained by the youngest pre-collapse Planchón age, which is  $49 \pm 14$  ka [[Klug et al. 2022](#)]. Therefore, it is inferred that the Planchón western collapse occurred approximately at 48 ka BP.

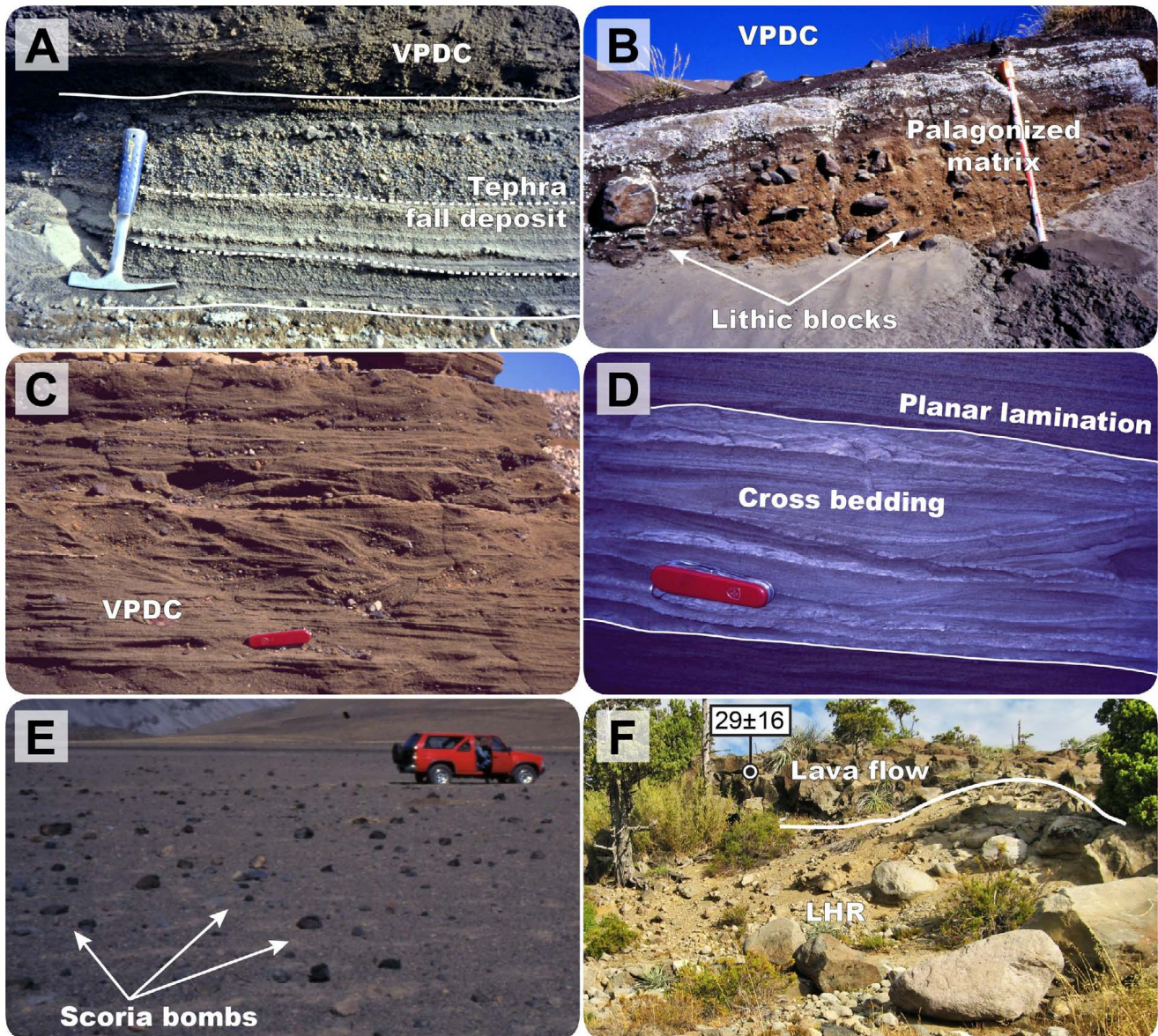


Figure 10: Holocene multiphase Valenzuela eruption deposits (see locations in Figure 9). [A] Tephra-fall deposit with three different units (see segmented lines). [B] Lithic blocks within a palagonized ash matrix in the proximal facies of the VPDC deposit, [C] and [D] Cross bedding and dune structures within the ashy matrix of the VPDC deposit (white lines). [E] Scoria bombs with cracked cauliflower-shaped surface, produced by hydroclastic cooling, on the surface of the Los Ciegos laminar flow deposit at El Peñon creek. [F] Younger lahars partially covering the post-collapse lava flow of Planchón near Los Mineros Creek, 22 km W from the source.

## 5 HOLOCENE DEPOSITS

### 5.1 Holocene multiphase Valenzuela eruption deposits

As previously mentioned, the Holocene multiphase Valenzuela deposits originated from the most explosive Holocene eruption of the Planchón volcano (Figure 9) that occurred approximately 7 ka BP, given by  $^{14}\text{C}$  dates [Naranjo et al. 1999; Naranjo and Haller 2002]. Our new observations include a revised field-based constraint of the deposit distribution, in addition to detailed stratigraphic descriptions of the basal tephra fall deposit and a facies-based characterization of the overlying PDC sequence. The overall sequence has been already recog-

nized by Naranjo et al. [1999] and Naranjo and Haller [2002] as sourced from a single eruption. Based on new stratigraphic observations of the different facies—each one associated with a single phase of this eruption—as well as their textural features, we reinterpret and reconstruct the eruptive phases as corresponding to an initial tephra-fall phase (Figure 10A), followed by the emplacement of extended pyroclastic dilute PDC (Figure 10B–D), and finally ending with a laminar PDC (Figure 10E).

The bottom of the sequence is recognized along the southern flank of the Valenzuela River, 12 km southeast of the Planchón volcano. It corresponds to a 30 cm-thick tephra fall

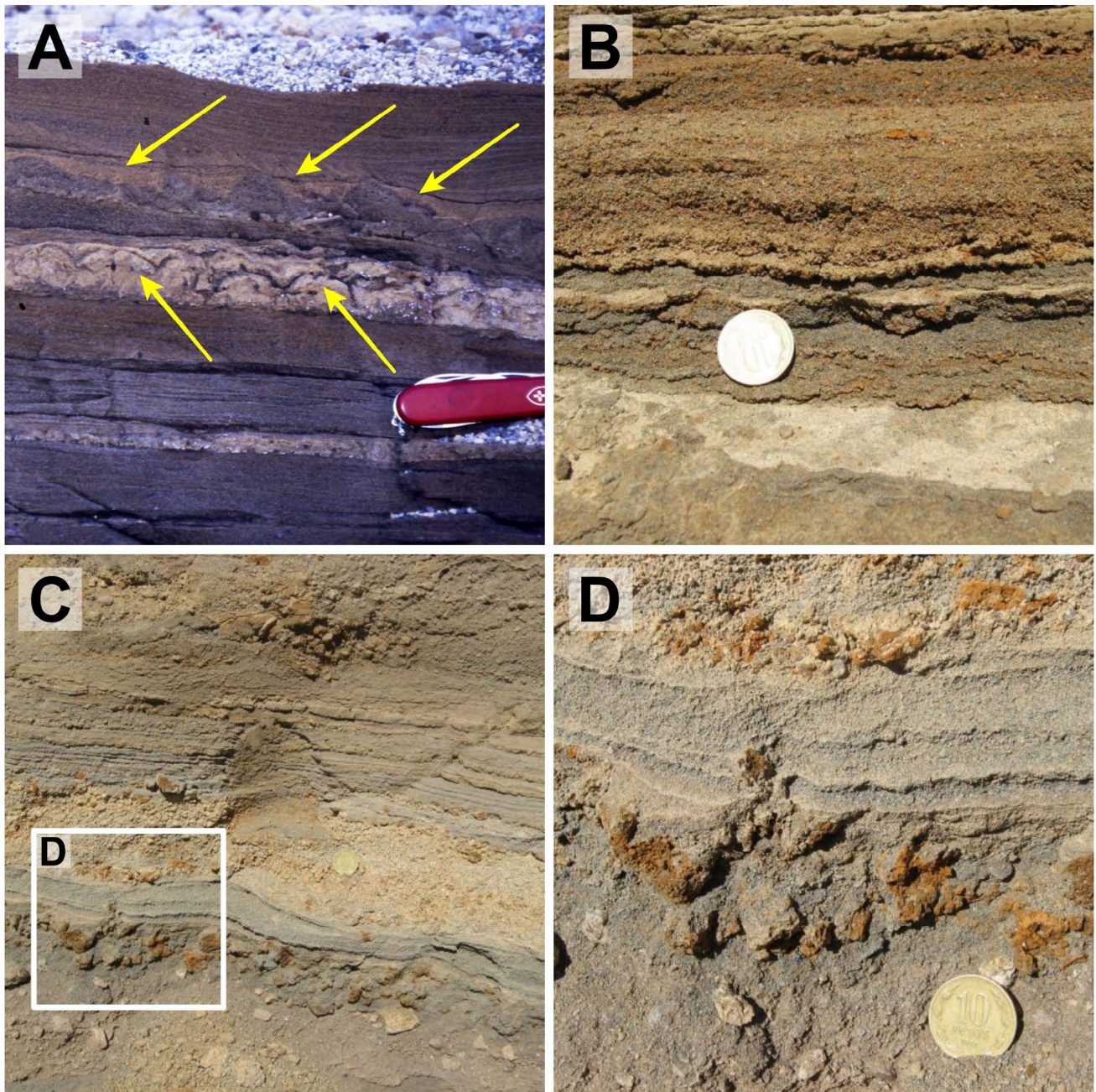


Figure 11: Medial facies of the Valenzuela dilute PDCs. [A] Soft-sediment deformation structures (yellow arrows). [B] Widespread palagonization of particles within laminated beds. [C, D] Palagonized juvenile scoria.

deposit (Figure 10A), composed of low-SiO<sub>2</sub> andesitic lapilli size scoria and dense juvenile fragments, which is organized in three different units (Table 4).

The middle unit is a dark-to-medium gray finely laminated ash deposit (Figure 10C–D; Table 4) that is recognized only on the Planchón's eastern flank and over the remnants of the Petoeroa volcano to the southeast as well as downstream valleys. The deposit has been denominated Oleada Piroclástica Valenzuela by Naranjo et al. [1999] and Naranjo and Haller [2002]. Some of the most relevant textural features correspond to the frequent occurrence of soft sediment deformation structures, well-developed lamination, palagonization of the ashy matrix

and juvenile clasts, and the existence of vesicles in the deposit (Table 4; Figure 11). We now refer to this deposit as "Valenzuela dilute PDC," whose revised distribution covers an area of c. 59 km<sup>2</sup>; it reached up to 12 km to the northeast (Vergara Valley) and 20 km to the southeast (Valenzuela Valley) from its source. Considering an average thickness of 18 m, its total volume is here estimated to be c. 1.12 km<sup>3</sup>.

The uppermost volcanic unit corresponds to Los Ciegos laminar PDC deposit (Figure 10E; Table 4), which covers an area of c. 12 km<sup>2</sup> on the eastern flank of the Planchón volcano, up to the Los Ciegos River. Its volume is estimated to have reached 0.012 km<sup>3</sup>. Haller and Risso [2011] based on Espizua

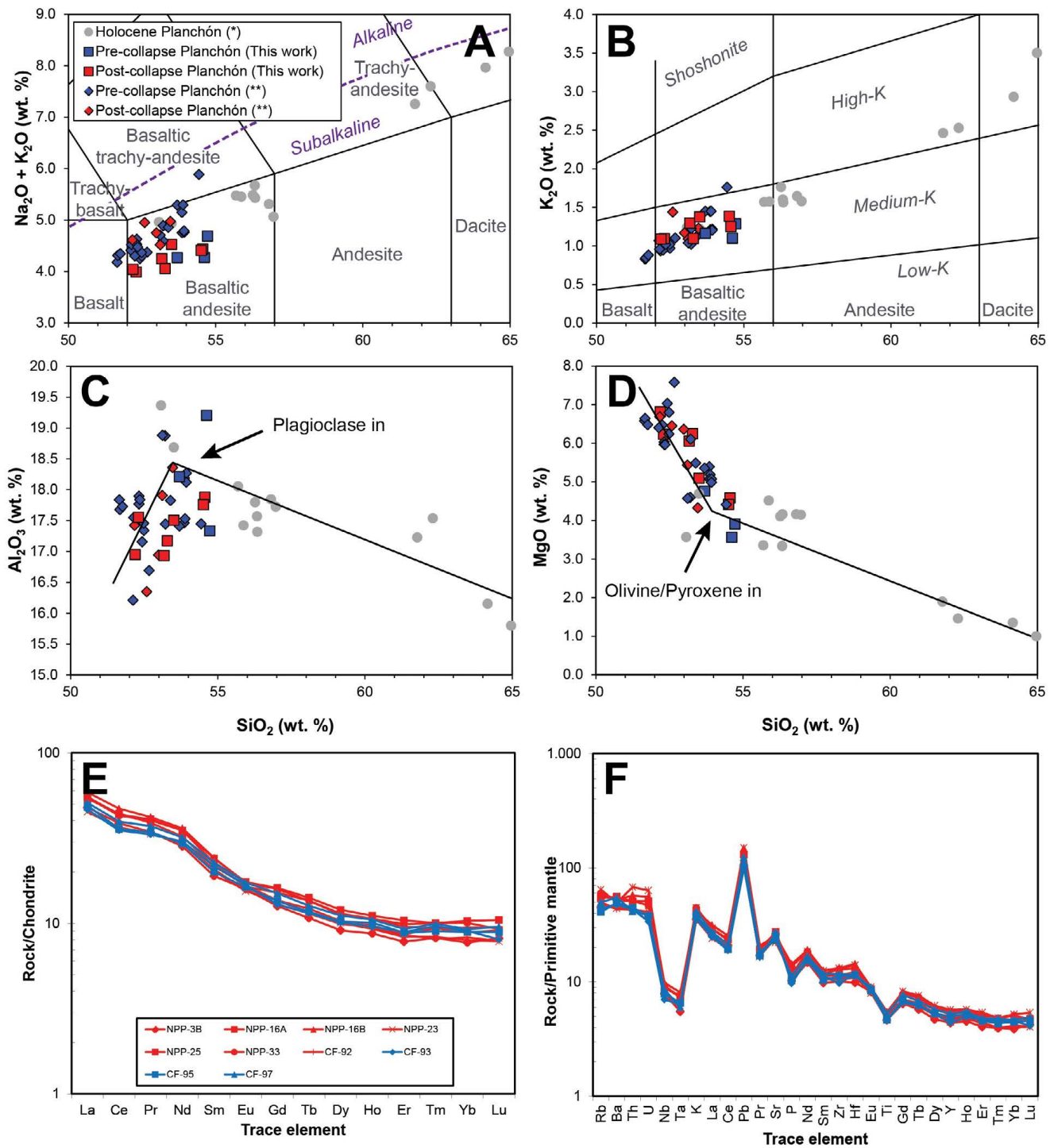


Figure 12: Geochemistry of the selected samples of Planchón volcano. [A] Total Alkali vs.  $\text{SiO}_2$  diagram [Le Maitre et al. 2002]. [B]  $\text{K}_2\text{O}$  versus  $\text{SiO}_2$  diagram [Peccherillo and Taylor 1976]. [C] and [D] are Harker diagrams of  $\text{Al}_2\text{O}_3$  and  $\text{MgO}$  vs.  $\text{SiO}_2$ , indicating the crystallization of plagioclase and olivine/pyroxene, respectively. [E] and [F] represent both primitive mantle- and REE-normalised diagrams [Sun and McDonough 1989]. The samples with (\*) are those from Naranjo and Haller [2002], and those with (\*\*) are from Tormey et al. [1995].

[2000] suggested that the Valenzuela PDC overlies till deposits representative of an Early Holocene glaciation (Paso Laguna Drift) and is locally covered by another glacial advance (Teno Drift) that divides it from Los Ciegos PDC. However, no clear mention is made of Los Ciegos PDC or any equivalent volcanic

unit, and no data on its stratigraphic position with respect to the so-called Teno Drift can be deduced from the original Espizua data. Therefore, in the light of the available evidence, there is no indication to interpret a stratigraphic gap between the Valenzuela and Los Ciegos units.

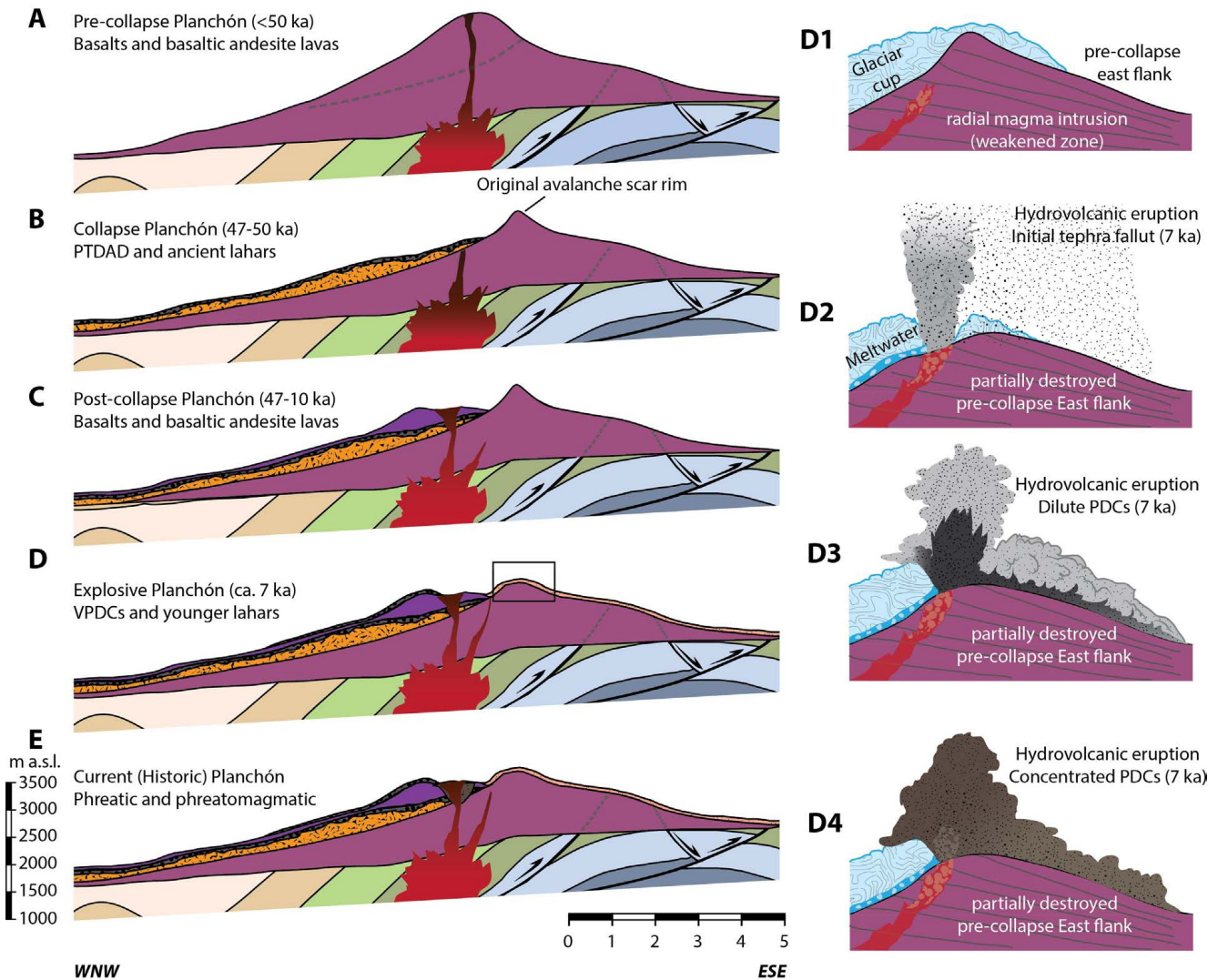


Figure 13: Cross-section cartoon of the morphologic and stratigraphic evolution of Planchón volcano. The PTAD is represented in orange, and the lahars are in dark grey. The basement structure is interpreted from the geology exposed north and south of the Planchón-Peteroa volcanic complex [Mosolf et al. 2019]. Insets from [D1] to [D4] show the chronologic deposition of the deposits associated with the Holocene multiphase Valenzuela eruption. The geometry of the plumbing system is schematic.

## 5.2 Lahar deposits

Holocene lahar deposits are found up to 15 km downwards along Claro River towards the west. These deposits overlie post-collapse lava flows and correspond to coarse debris from pebble-sized up to 5 m diameter boulder-blocks, locally forming mid-channel bars, with coarse sand to gravel size loose matrix (Figure 10F). These deposits were formed at the expense of local morainic arches up to 30 m high and, during their transit, generated remarkably striations on Post-collapse Planchón lavas (Figure 2).

## 6 GEOCHEMISTRY

Both pre- and post-collapse lavas from Planchón correspond to monotonous basalts and contain 10–45 % phenocrysts with a mineral assemblage consisting of plagioclase (70–80 %) + olivine ± clinopyroxene and few oxides. Only slight variations are observed between both edifices, mainly related to an

increase of olivine and clinopyroxene from 3 up to 5 % in the younger one [Tormey et al. 1995].

All the lavas are sub-alkaline basaltic andesites, displaying a narrow  $\text{SiO}_2$  content (52.2–54.7 wt. %; Figure 12A) and medium-K (1.1–1.4  $\text{K}_2\text{O}$  wt. %; Figure 12B). These rocks are clearly distinguished from samples of Peteroa-Azufre volcanoes, which show a wider composition with high-K andesites and dacites (Figure 12A).  $\text{Al}_2\text{O}_3$  and MgO display incompatible trends up to 54 wt. %  $\text{SiO}_2$  when plagioclase and olivine/pyroxene crystallize (Figure 12C, D). Despite the bulk composition being relatively homogeneous, pre-collapse lavas are slightly more evolved than the post-collapse ones (with a decrease from 54.4 to 53.4 wt. % of  $\text{SiO}_2$  in their average composition, respectively). Other compositional changes support this observation; the increase of Mg# from 47.3 to 53.8, an increase of  $\text{CaO}/\text{Al}_2\text{O}_3$ , and a decrease in  $\text{FeO}_T/\text{MgO}$  from 2.0–1.7 in the post-collapse products to 0.46–0.48 (Table 5).

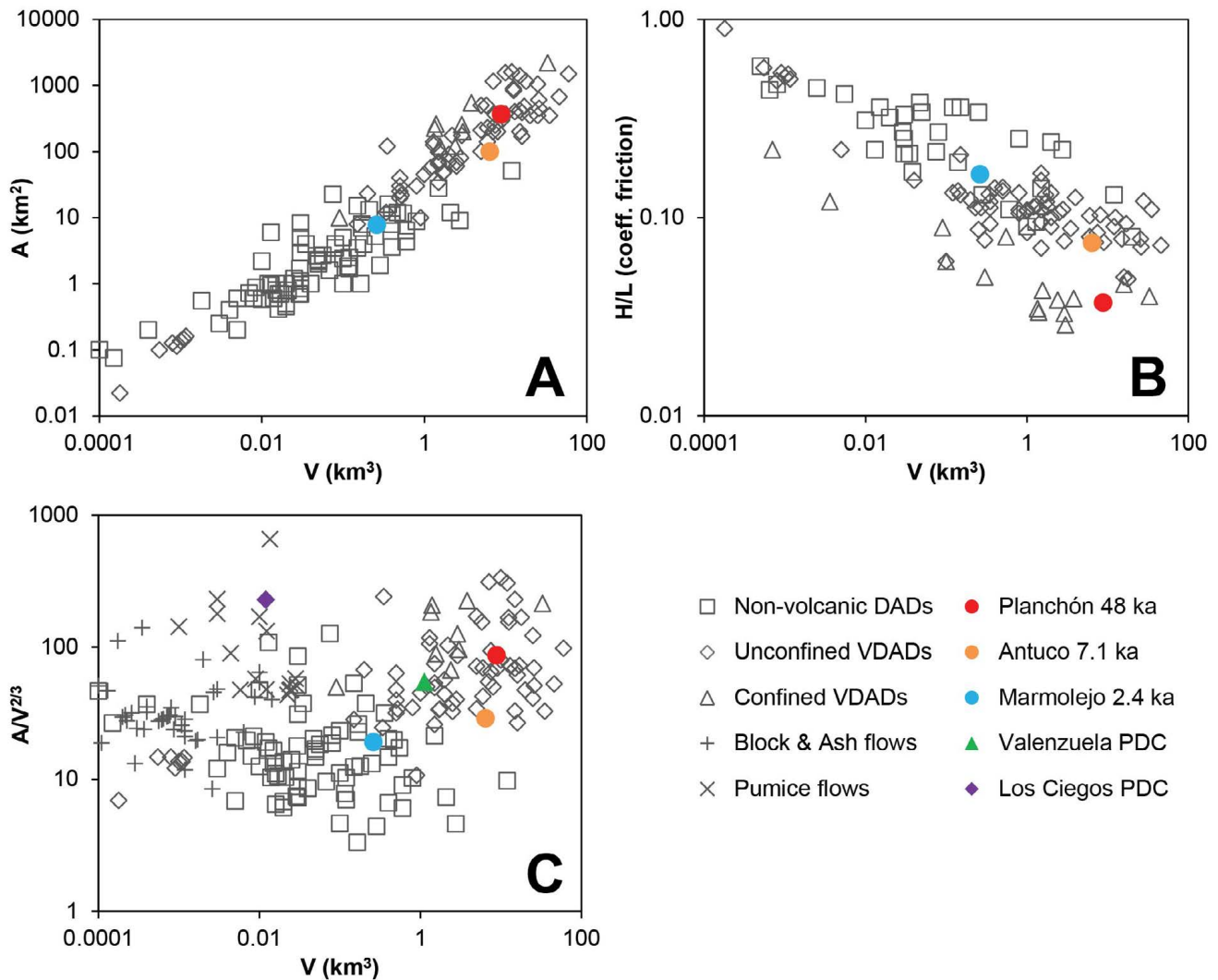


Figure 14: Size [A] and mobility parameters [B] of the Planchón 48 ka debris avalanches in relation to non-volcanic landslides (DADs) and subaerial volcanic landslides (confined and unconfined VDADs) reported by Tost et al. [2014]. [C] The Valenzuela and the Los Ciegos PDCs are compared to other block-and-ash and pumice flows also reported by Tost et al. [2014]. The Antuco 7.1 ka [Romero et al. 2022] and Marmolejo 2.4 ka [Melo et al. 2022] debris avalanches are also plotted for comparison.

Large enrichment in La (Light Rare Earth, LREE) is evidenced in basaltic andesites of the post-collapse Planchón, while moderate enrichment is observed in other LREE such as Pr and Sm (Figure 12E). The Middle Rare Elements (MREE; Eu, Gd, Tb, Dy, and Ho), as well as Heavy Rare Elements (HREE; Er, Tm, Yb, and Lu) display discrete-to-moderate enrichments for the primitive mantle. Some compatible trace elements (i.e. Sr, Ni, Cr, Sc, and Zn) show a sharp difference between the pre-and post-collapse rocks (Figure 12; Table 5). On the other hand, Large Ion Lithophile Elements (i.e. Rb, Ba, and Pb), which behave as incompatible, display constant concentrations along all the samples. High Field Strength Elements (i.e. Th, U, Nb, Zr, and Hf) do not exhibit significant variation during the different stages of edifice evolution (Figure 12F; Table 5).

As shown in Figure 12F the pattern of incompatible elements shows positive anomalies for K and Pb, while Ti, Nb, and Ta show negative anomalies; additionally, small positive

anomalies for Nd, Sm, and Ba are observed. Comparatively, post-collapse lavas display higher positive anomalies of Rb, Th, U, and Hf in contrast to the pre-collapse Planchón (Figure 12F).

## 7 DISCUSSION

### 7.1 Planchón – a monotonous mafic volcano

Our data, combined with that published in the literature, indicate no significant difference in the composition between the pre-and post-collapse magmas from Planchón volcano, despite the pre-collapse samples being slightly more evolved than the post-collapse. This modest difference can be explained by the relatively small number of analyses considered or by differences in the loss of ignition between diverse samples. The pre-collapse samples display a slightly wider trace element variability that can also be explained by the small number of samples analyzed. Higher Cr and Ni abundances

Table 1: Comparison and correlation of the different stratigraphic units described by [Tormey \[1989, 2010\]](#), [Tormey et al. \[1995\]](#), [Naranjo et al. \[1999\]](#) and [Naranjo and Haller \[2002\]](#), and this work.

Stage	In <a href="#">Tormey [1989]</a> and <a href="#">Tormey et al. [1995]</a>	In <a href="#">Naranjo et al. [1999]</a> and <a href="#">Naranjo and Haller [2002]</a>	In <a href="#">Tormey [2010]</a>	This work
Holocene Planchón	Known as Peteroa: Holocene age; volume <1 km <sup>3</sup> ; composition between 55 and 69 wt. %SiO <sub>2</sub> .	Known as Planchón 3: Age <14 ka; products totalize 0.14 km <sup>3</sup> ; composition between 55 to 69 wt. % SiO <sub>2</sub> .	Known as Peteroa: It considers from the 7 ka eruption to the present. Magmas fed from shallow-crust levels, underwent magma mixing and produced more evolved compositions.	Known as Holocene Planchón: Age <14 ka; products totalize 1.14 km <sup>3</sup> ; compositions 55 to 60 wt. % SiO <sub>2</sub> .
Post-collapse Planchón	Known as Planchón II: Edifice of 5 km <sup>3</sup> ; composition between 52 and 55 wt. %SiO <sub>2</sub> .	Known as Planchón 2: Age Late Pleistocene, deeply glaciated. Edifice. of 3.5 km <sup>3</sup> ; composition between 52 and 54 wt. % SiO <sub>2</sub> .	Known as Planchón II: Edifice of 5 km <sup>3</sup> ; Age: Holocene. Basalt and basaltic andesite lavas sourced from mid-crustal depths.	Known as post-collapse Planchón. Maximum 46.5 ± 10.4 ka and 29 ± 16 ka concordant ages and minimum 14 ka. Edifice of 3.5 km <sup>3</sup> ; compositions of 52 to 55 wt % SiO <sub>2</sub> . Volume of 8.2 ± 1.2 km <sup>3</sup> ; minimum age constrained to 46.5 ± 10.4 ka and 29 ± 16 ka from radiometric ages of overlying lavas; maximum the 49 ± 14 ka lava-age given by <a href="#">Klug et al. [2022]</a> .
Planchón-Teno Debris Avalanche	Deposit of 9 km <sup>3</sup> ; age of 9 ka based on date on wood by <a href="#">MacPhail [1973]</a> . Relates the collapse with pumice deposits to the east.	Volume: >10 km <sup>3</sup> ; Age: 12 ka after Hauser (1990, 1994), but authors suggested Upper Pleistocene age.	Known as Rio Teno Debris Avalanche; ca. 10 km <sup>3</sup> ; age: 11 ka; run out 95 km and H/L of 0.03.	Known as post-collapse Planchón. Maximum 46.5 ± 10.4 ka and 29 ± 16 ka from radiometric ages of overlying lavas; maximum the 49 ± 14 ka lava-age given by <a href="#">Klug et al. [2022]</a> .
Pre-collapse Planchón	Known as Planchón: edifice of 25 km <sup>3</sup> ; composition between 51 and 55 wt. %SiO <sub>2</sub> .	Known as Planchón 1: Age: Pleistocene, deeply glaciated; edifice of 25–30 km <sup>3</sup> ; composition between 51 and 53 wt. % SiO <sub>2</sub> .	Known as Planchón: edifice of 43 km <sup>3</sup> ; age between 14 and 11 ka. Basalt to basaltic andesite in composition.	Known as Planchón or pre-collapse Planchón. New ages of 191 to 49 ka from <a href="#">Klug et al. [2022]</a> and this work; compositions of 51 to 55 wt. % SiO <sub>2</sub> .
Peteroa-Azufre	Known as Azufre: Edifice of 30 km <sup>3</sup> ; age <0.55 Ma; composition of 52 to 66 wt. % SiO <sub>2</sub>	Known as Peteroa-Azufre; edifice up to 68 km <sup>3</sup> ; age: between 1.2 and 0.55 Ma; composition between 51 and 65 % SiO <sub>2</sub> .	Known as Volcan Azufre (69 km <sup>3</sup> ): a long-lived polycyclic basaltic andesite to dacite stratovolcano, younger than 0.55 Ma.	Known as Peteroa-Azufre. New ages of ~300 to 150 ka from <a href="#">Klug et al. [2022]</a> .

in the post-collapse Planchón may also result from a higher accumulation of olivine, as previously reported for these samples [[Tormey et al. 1995](#); [Holbik 2014](#)]. Positive anomalies for K and Pb and negative Ti, Nb, and Ta are typically observed in arc magmas due to a metasomatized mantle wedge and Fe-Ti oxide fractionation (in the case of Ti). Positive anomalies of Rb and Th have been previously interpreted as a result of higher degrees of crustal contamination at either upper or lower crustal levels [e.g. [Tormey et al. 1995](#)].

Nevertheless, all these trace element patterns are the same for all the Planchón samples; so essentially, they were produced by the same magmatic processes during the long-term evolution of the system. Therefore, the mafic lavas erupted by Planchón before and after the collapse do not indicate any substantial change in the magma composition, pointing to a monotonous production of basalt. This new finding contradicts the hypothesis of [Tormey et al. \[1995\]](#) who identified that magma storage may have changed from a mid-crust re-

Table 2: Lithology, sedimentology, and geomorphology of the Planchón-Teno debris avalanche deposit (PTDAD).

Facies	Lithology, sedimentology, and geomorphology
Distal Matrix facies >40 km WNW	Clastic, matrix-supported indurated deposit, containing dark gray or brown subrounded volcanic clasts, 5 to 30 cm $\phi$ . The matrix is pale gray to brown, with a mean fine-to-medium sand grain size, 14 to 24 % silt and clay and nearly 10 % of subangular to subrounded volcanic clasts of 1 to 4 cm $\phi$ . At a railroad cut outcrop (southern margin of Convento Viejo lake) the observable deposit is 4-5 m thick and contains elongated, partially cohesive subrounded blocks up to 1.3 m long, while the matrix is composed of fine sand and clear gray color. It includes clastic dark gray to reddish lithic fragments of volcanic and granitic origin up to 20 cm $\phi$ , which are organized in domains with variable matrix/clast ratios. The hummocks are abundant in this portion of the deposit and may reach up to 20-30 m-length and ca. 10 m high. Internally, they consist of metric blocks of lava surrounded by a whitish, clay-rich interclast matrix. The interclast matrix is brown-reddish or gray.
Medial Mixed and highly tritirated 25–40 km NW	In P0221, the deposit is at least 15 m-thick, matrix supported, with clear gray color and indurated. The matrix consists of fine sand-to-gravel size, with white to gray color domains, and supports fresh-likely basaltic blocks. These blocks grade upwards in the deposit, with subrounded oblate shapes and size up to 1.5-2.0 m and faint imbrication from east to west. Some accidental clasts are also recognized. Some hummocks identified in P0121 include highly tritirated blocks within the gray matrix. These blocks are subrounded, sometimes prolate, and reach up to 12 m $\phi$ , with a core composed of tritirated subrounded to angular clasts (centimetric to metric size) immersed within an autoclastic matrix. Some blocks are reddish, less cohesive and reach a few meters in size. The interclast matrix includes polymictic fragments from sand-to-gravel size, with similar composition to that of the blocks. Apparently, the finer matrix material is derived from the deep fragmentation of non-cohesive blocks. At 4.6 km ESE of P0221, the ca. 20 m thick outcrop is made of 10-40 cm $\phi$ angular-to-rounded gray porphyritic basaltic andesite clasts, some of them vesicular. Some subrounded accidental clasts reach 2 m $\phi$ and were ingested from the Cenozoic basement. The PTDA deposit is partially eroded by subsequent alluvial deposits.
Proximal Mixed facies <25 km W	The avalanche is generally >20 m thick (base not observed) made of a pale gray to white fine-grained matrix, containing dark-gray or reddish subangular volcanic clasts with size varying from 0.2 to 7 m $\phi$ ; in addition, the avalanche contains decametric oblong decametric clasts made of undisturbed lava sequences. Some of these lavas develop hackly joints. The proximal deposits show natural exposures up to 20-35 m, mainly at erosive terraces of the Claro River. Within the sequence and overlying the PTDAD, a series of poorly sorted clastic deposits with gray matrix contain subrounded clasts up to 2 m size.

Table 3: Groundmass  $^{40}\text{Ar}/^{39}\text{Ar}$  plateau and unspiked K-Ar (\*) ages of Planchón volcano selected samples (ka).

Sample ID	UTM (N)	UTM (E)	Lithology	Age	Analytic $2\sigma$ error
CF92	6107882	346371	Subaerial hackly jointed basalt overlying the PTDAD	29	16
NPP-33	6110323	341366	Subaerial hackly jointed basalt overlying the PTDAD	46.5*	10.4
CF97(a)	6102535	361778	Pleistocene basaltic block in moraine	100	40
CF97(b)	6102535	361778	Pleistocene basaltic block in moraine	110	30
CF93	6107936	346335	Subaerial hackly jointed basalt underlying the PTDAD	120	30

gion (12–18 km), to shallower levels (c. 3 km depth) just prior the lateral collapse; these authors suggested this condition may have ultimately triggered the lateral collapse. Contrary to what these authors mentioned, Holocene eruptions include more silicic compositions ranging from basaltic andesites to PDC-dacite pumice (Figure 12A) with high K signature (Figure 12B),

as well as trachyandesites that erupted in the 2018/19 eruption [Naranjo and Haller 2002; Romero et al. 2021] that suggest a different petrological evolution and possibly pre-eruptive storage.

Table 4: Summary of the descriptive characteristics of Holocene multiphase Valenzuela eruption deposits.

Eruption deposits	Age
Basal tephra fallout	
<p><b>Basal unit (7 cm thick):</b> consists of reversely graded fine-to-medium lapilli containing c. 15 % dark gray to brown scoria, 10 % angular hydrothermally altered lithics, and 75 % gray subrounded to subangular lithics. At c. 2 cm from the base a 0.5 cm-thick fine ash layer interrupts the bed.</p> <p><b>Middle unit (11 cm thick):</b> consists of a series of lithic-rich tephra intercalating cm-thick coarse ash layers with medium-to-coarse lapilli layers.</p> <p><b>Uppermost unit (12 cm thick):</b> correspond to a reversely graded, medium-to-coarse lapilli bed containing c. 30 % brown subrounded pumice clasts, c. 25 % dark gray dense subangular juvenile fragments, c. 20 % hydrothermally altered angular fragments and c. 25 % angular lithics. The top of the sequence contains some scoria clasts up to 2 cm diameter.</p>	AMS dating on overlying colluvial deposits yields ages of $7010 \pm 70$ BP [Naranjo et al. 1999]
Valenzuela dilute PDC	
<p><b>Proximal facies (60–80 m thick):</b> Outcrop in the inner walls of the Planchón avalanche caldera and consist of remarkable PDC sequences showing planar stratification and very low angle cross stratification, as well as festooned erosion channels from 60 to 10 cm, in tilted proximal facies and more distal horizontal facies, respectively.</p> <p><b>Medial facies (3–10 m thick):</b> Recognized between 7 and 10 km to the north and east, include up to 40 cm lava blocks, immersed in the surged matrix ashes. Locally, up to 30 cm-thick palagonized ash layers are interbedded with layers of thick gray ash supporting palagonized medium-to-coarse brown lapilli scoria. Occasionally light-gray ash and laminated coarse ash to fine lapilli (50 % lithic and 50 % palagonized scoria) is observed. Some of them are plastically deformed.</p> <p><b>Distal facies (&lt;8 m thick):</b> These are composed of medium-gray coarse lapilli and ash; include accidental lava-blocks and cobbles up to 20 cm. Sigmoidal beds and lenses 2 to 20 cm thick and 40 cm long are compound of angular, medium-to-coarse lapilli-size lithics. Light brown fine ash beds are also present and plastically deformed. They are rich in water vapor vesicles and have low-angle truncations both below and above. Climbing dunes and small erosion channels are visible.</p> <p><b>Terminal facies (&lt;4 m thick):</b> These directly overly the tephra-fall deposits from the first eruptive phase. They are constituted by layers interbedded with accidental fine regolith materials and soil. Indeed, surge accumulations of up to 50 cm are observed there (Figure 3), with 3 cm-thick and 2.5 m-long lenses, interbedded with 20 to 50 cm-thick of disturbed regoliths.</p>	AMS dating on bioturbation structures yields ages of $7030 \pm 70$ and $7020 \pm 60$ BP [Naranjo et al. 1999]
Los Ciegos laminar PDC	
<p>Chaotic, matrix-supported and poorly sorted deposit up to 2 m thick deposit, consisting of matrix supporting centimeter-sized bombs. The matrix is formed of scoriaceous lapilli and ash and contains sub-angular to sub-rounded juvenile and lithic fragments, with subordinate hydrothermally altered fragments. The finer fractions show enrichment in free crystals of plagioclase and magnetite, as well as dark glass shards. The juvenile scoria clasts are black and show vesicular and glassy textures, with little (&lt;5 %) crystal content of plagioclase, olivine, and orthopyroxene, on a dark and opaque matrix, weakly altered to palagonite. The juvenile bombs (c. 5 %) are cauliflower in shape reaching up to 30 cm diameter and displaying a ragged glassy surface. The proximal facies constitute a thin surface directly above the Valenzuela dilute PDC. It forms a plain between the lower flank of the volcano and the Los Ciegos River. From there, it thins out towards the distal sectors, on the western bank of the river.</p>	Not available. Presumably, the final phase of the same eruption forming the Valenzuela deposit.

## 7.2 Tectonic controls on magma ascent

The complex structural network in PPVC (Figure 1) should be considered a first-order factor in controlling magma ascent and storage. For instance, EEFS is suggested to play a critical role in compartmentalizing magma-derived hydrothermal fluids to the east of the fault plane (in the PPVC area), where the

fault zone acts as a barrier to cross-fault fluid migration and channels fault-parallel fluid flow to the surface from depth [Pearce et al. 2020]. Tibaldi et al. [2010] indicates that, in such contexts, magma is transported beneath the volcano to the surface along the main faults. Bonali et al. [2013] assumed the magma pathways dip  $45^\circ$  west for volcanoes that overlie thrust faults, as Planchón. On the other hand, Tormey [2010]

Table 5: Bulk rock geochemistry of Planchón volcano selected samples, for major (in wt%) and trace elements (in ppm).

Sample	NPP-3B	NPP-16A	NPP-16B	NPP-23	NPP-25	NPP-33	CF-92	CF-93	CF-95	CF-97
Age (ka)						46.5 ±10.4	29 ±16	120 ±30		100 ±40 110 ±30
SiO <sub>2</sub>	50.83	53.31	51.53	50.63	52.85	52.09	52.25	53.28	52.82	53.51
TiO <sub>2</sub>	1.01	1.04	1.19	1.11	1.03	1.14	1.01	1.02	1.01	1.15
Al <sub>2</sub> O <sub>3</sub>	17.06	17.47	16.41	16.44	17.22	17.04	16.84	18.74	17.91	16.95
Fe <sub>2</sub> O <sub>3</sub>	9.49	8.36	9.59	9.73	8.72	9.38	9.23	7.96	8.87	9.51
MnO	0.16	0.14	0.15	0.16	0.14	0.15	0.15	0.14	0.15	0.16
MgO	6.06	4.47	5.87	6.61	4.28	4.96	6.13	3.48	4.68	3.82
CaO	8.48	8.31	7.74	8.16	8.18	7.89	8.24	8.57	8.5	7.85
Na <sub>2</sub> O	2.81	3.12	2.86	2.86	2.93	3.07	2.9	3.09	3.05	3.32
K <sub>2</sub> O	1.07	1.22	1.26	1.06	1.34	1.34	1.08	1.07	1.15	1.26
P <sub>2</sub> O <sub>5</sub>	0.22	0.26	0.31	0.25	0.25	0.3	0.23	0.21	0.22	0.25
Total	97.18	97.71	96.91	97	96.95	97.35	98.06	97.55	98.37	97.77
Sc	28	29	26	27	28	27	26	25	27	28
V	236	231	232	244	235	238	235	232	237	275
Cr	126	82	158	256	54	79	176	49	67	32
Co	34	26	32	37	26	30	34	20	28	26
Ni	70	29	72	88	20	49	82	12	35	13
Zn	87	84	94	92	86	93	88	81	84	91
Ga	19	20	20	19	19	20	19	21	21	21
Rb	29	35	36	30	41	38	32	28	26	32
Sr	556	576	533	539	470	513	514	568	525	492
Y	20	22	24	20	26	25	21	20	23	24
Zr	113	128	149	118	148	145	115	109	125	131
Nb	5.6	6.4	7	5.9	6.4	6.6	5.8	5	5.6	6.1
Ba	323	388	363	309	345	359	304	331	344	384
La	17.5	19.8	21.6	16.5	20.2	20.1	16.8	17	18	18.7
Ce	37	42.1	45.1	34.9	41.6	41	34.8	33.6	34.2	37.8
Pr	4.7	5.33	5.75	4.6	5.58	5.51	4.65	4.55	4.71	5.1
Nd	20.1	23	25.7	21.1	25	25	20.9	21.5	21	23
Sm	4.38	5.01	5.6	4.69	5.55	5.23	4.79	5	4.63	5.27
Eu	1.38	1.45	1.5	1.34	1.52	1.43	1.36	1.47	1.41	1.51
Gd	3.87	4.17	4.86	4.19	4.93	4.63	3.97	3.94	4.14	4.6
Tb	0.62	0.71	0.79	0.66	0.82	0.79	0.66	0.67	0.68	0.74
Dy	3.47	3.94	4.28	3.83	4.57	4.34	3.78	3.86	3.91	4.23
Ho	0.74	0.83	0.91	0.79	0.94	0.91	0.81	0.81	0.86	0.89
Er	1.95	2.15	2.38	2.08	2.59	2.47	2.12	2.22	2.19	2.3
Tm	0.29	0.33	0.33	0.3	0.36	0.36	0.29	0.34	0.32	0.35
Yb	1.91	2.2	2.34	1.98	2.57	2.5	2.06	2.24	2.21	2.29
Lu	0.31	0.35	0.36	0.3	0.4	0.35	0.3	0.31	0.34	0.36
Hf	3.06	3.77	4.44	3.65	4.32	4.06	3.42	3.64	3.55	3.56
Ta	0.23	0.3	0.33	0.24	0.31	0.3	0.24	0.26	0.27	0.25
Pb	7.51	9.24	10.49	7.75	10.64	9	7.19	7.67	7.15	8.78
Th	3.63	4.33	4.88	3.65	5.75	4.38	3.68	3.67	3.79	3.54
U	0.79	1.07	1.17	0.87	1.33	0.98	0.84	0.71	0.79	0.81

assumes that much of the development of the volcanic PPVC is likely to have been in a neutral state of stress in the crust, transitional from compression to extension, as a result of the intersection of the volcanic arc with extensional basins to the east. As in other reverse fault systems, fault conjugation can facilitate magma ascent [Naranjo et al. 2018].

During the Late Miocene-Early Pliocene, these east-vergence reverse faults favored the ascent and evolution of dacitic and dioritic intrusive bodies [Piquer et al. 2010]. Moreover, their intersection with major NW-SE faults constitutes high-permeability and structural damage zones [Vigide et al. 2020] characterized by upper-crustal seismic clusters, Neogene

intrusive complexes, giant porphyry Cu-Mo deposits, and active volcanic centers [Piquer et al. 2019; Pearce et al. 2020]. This kind of structural arrangement is also observed in the Central Andes, where major fault systems encase minor faults and fracture meshes or domains controlling the emplacement timing of the magmatic systems acting as pulsatile suction bombs [Naranjo et al. 2018].

The recent shallow level seismicity of the area includes earthquakes of moderate to large magnitude [e.g. Vigide et al. 2020] such as that of MW 6.5 on August 28, 2004, which occurred at a depth of 5 km, with an epicenter 8 km north of the volcano [Naranjo and Welkner 2004; Comte et al. 2008], and the MW 5.2 event on March 1, 2010, which occurred at a depth of 13.4 km, with an epicenter located 9 km SE of the vent [SERNAGEOMIN 2010]. This MW 5.2 seismic event also suggests an interplay between large interplate earthquakes and the displacement of the structural network below the volcanic arc; it occurred just two days after the MW 8.8 Maule megathrust earthquake (epicenter c. 195 km SW from the volcano), which ruptured a 500 km-long segment of the plate interface [Ruiz and Madariaga 2018]. In addition, several arc volcanoes parallel to the 2010 rupture zone, including Planchón, experienced subsidence up to 15 cm, whereas the upper crust showed generalized east–west tension [Pritchard et al. 2013].

In the case of Planchón, this deformation was concentrated southwest from the active vents and ten months after an eruption occurred [Haller and Risso 2011; Naranjo 2012; Aguilera et al. 2016]. The area of the Maule earthquake experienced two significant previous historical events in 1835 and 1751, whereas marine terraces formed over the last c. 80 ky at mean rates of  $0.50 \text{ m ka}^{-1}$  along the Maule rupture zone indicate long-lived coastal uplift correlated to persistent offshore earthquakes along this segment [Jara-Muñoz et al. 2017]. Hence, Maule-type megathrust earthquakes should have occurred several times in the last c. 50 ky in this area, producing cyclic relaxation along the nearby arc segment. This condition should have facilitated temporary crustal compression-relaxation as an upper crustal bombing system driving a steady supply of dense, mafic magma through these crustal damage zones to feed the activity of Planchón efficiently.

### 7.3 Edifice growth and instability factors

Mafic (i.e. basaltic and basaltic andesite) stratovolcanoes display higher eruption rates and short-lasting evolutions than intermediate-composition volcanoes (i.e. andesitic or dacitic [e.g. Hildreth et al. 1998]). Mafic stratovolcanoes flanks tend to approach the repose angle ( $33\text{--}36^\circ$ ) and are more frequently affected by dike emplacement and fissure eruptions that increase edifice instability by mass/heat transfer or pore pressure rise [e.g. Walker 1993; Baloga et al. 1995; Elsworth and Voight 1996; Hildreth et al. 1998; Elsworth and Day 1999; White et al. 2006; Romero et al. 2021]. Rapid growth and subsequent collapse have been widely observed at basaltic and basaltic andesite volcanoes in arc settings [e.g. Ponomareva et al. 2006; Romero et al. 2021; Valverde et al. 2021].

Among the hypotheses on the conditioning and triggering factors leading Planchón to collapse, Tormey et al. [1995] proposed a change in the source depth of the magma storage zone

related to the temporary development of a shallow magma body (c. 3 km depth). In contrast, Naranjo et al. [1999] and Naranjo and Haller [2002] pointed to the rapid growth, gravitational instability, and the structural weakening of the basement below the volcano as the leading potential causes for the sector collapse. Other factors suggested by Tormey [2010] include hydrothermal activity, melting of the summit ice cap, or minor eruption.

The substratum lithology and structure may also contribute to instability as in other mafic volcanoes [e.g. Mathieu et al. 2011; Goto et al. 2019; McLeod and Pittari 2021; Romero et al. 2022]. To imagine the substratum morphology, we traced topographic profiles between the eastern and western volcano/basement mapped interface of pre-collapse Planchón (near Lagunas de Teno and by the middle of the edifice). Its surface corresponds to a tilted block dipping ca.  $7^\circ$  to  $17^\circ$  west (Figure 13A). Extending the ILCF and EFFF below the PPVC means this block is limited by these tectonic structures (Figures 1 and 13). The soft lithologies of the edifice substratum (i.e. Jurassic sandstones, limestones, and conglomerates) may also have played a role in contributing instability and edifice deformation as in other remarkable volcanic debris avalanche examples [van Wyk de Vries et al. 2000; van Wyk de Vries et al. 2001; Dufresne et al. 2010].

The size and rapid growth of Planchón represent another critical factor that would have promoted instability as hypothesised by previous works [Naranjo et al. 1999; Tormey 2010]. The best estimate for the volume of the whole PPVC is c.  $163 \text{ km}^3$  [Völker et al. 2011], and the sole volume of Planchón volcano ranges from  $30$  to  $50 \text{ km}^3$ ; these estimates consider a basal radius of 4.5 km, and a pre-collapse maximum height in the range of 1.5 and 2.5 km above its base. These heights consider the geometric projection of the Planchón 1 flanks (Figure 3A) and are realistic if compared to similar stratovolcanoes of the Transitional Southern Volcanic Zone (TSVZ) of the Andes [Tormey et al. 1991; Stern 2004; Stern et al. no date], such as Tupungato, San José or Maipo. Considering the maximum age of Planchón constrained by the latest eruptive products of Peteroa-Azufre ( $153 \pm 3 \text{ ka}$  [Klug et al. 2022]) and the age of the collapse around 48 ka BP, the minimum eruptive fluxes for pre-collapsed Planchón volcano was  $0.3$  to  $0.48 \text{ km}^3 \text{ ka}^{-1}$ . Despite a minimum estimate, this is among the higher eruptive rates of arc stratovolcanoes reported by Mixon et al. [2021], ranging from  $0.01$  to  $0.87 \text{ km}^3 \text{ ka}^{-1}$ . This evidence led us to support the hypothesis that rapid growth is the main factor for Planchón volcano instability.

On the other hand, Tormey [2010] argued that “glaciated volcanoes can increase sediment pore pressure by melting glaciers, which represents an ideal environment for flow formation from debris” [after Pierson et al. 1990; Miletì et al. 1991; Voight 1996]; however, this factor is not necessarily relevant in the formation of a debris avalanche from a sector collapse as it removes major fragments of the volcanic edifice [Siebert et al. 1987], but, as the Nevados del Ruíz 1985 case, two large lahars were triggered, after the rapid ice and snow cover melting. Deposits related to extensive lahars are common at the post-collapse Planchón. We do not support the ice melting as a first order factor contributing edifice instability due to the

scarcity of hydrothermally altered material in the avalanche matrix, clasts, and blocks that suggests the edifice did not undergo extensive hydrothermal weakness before the collapse. This argument rules out the possibility of an external factor, such as a glacial retreat, to have influenced the collapse.

#### 7.4 Avalanche mobility

Naranjo et al. [1997], Scott et al. [2001], and Tormey [2010] have estimated exceptionally high mobility for the PTAD, with a coefficient of friction between 0.03 and 0.04. Long-run-out debris avalanches are more likely to occur in settings where initially partly saturated collapsing masses move down deep valleys and become thoroughly liquefied at their base; a basal lubrication zone enhances flow mobility by reducing basal shear [Tost et al. 2014]. Basal lubrication occurs when pore water is available within the base of the flowing mass or in the sediments immediately below it. When entering the Claro River valley, the PTAD became highly confined and achieved a very low friction coefficient (Figure 14A). Also, an intense syn-transport fragmentation and crushing may have increased elastic energy between the larger particles and frictional reduction within the matrix favoring exceptional mobility [Perinotto et al. 2015]. In this respect, there is no need of external water entrainment [e.g. Tormey 2010] to explain such exceptionally high mobility.

The emplacement velocity for the PTAD can be estimated tentatively in absolute terms from its climbing ability, using the method of Francis and Baker [1977], which takes account of frictional losses by comparing the height descended with the maximum height climbed. The overall percentage of frictional loss ( $F$ ) for the Planchón-Teno avalanche was:

$$F = 100 \cdot \left[ 1 - \left( \frac{h}{H} \right)^{0.5} \right], \quad (1)$$

where  $h$  is the height gained and  $H$  the height loss. Considering the summit of the volcano as (a) 4200 to (b) 5200 m asl, two scenarios are visualized:  $H_a = 3539$  m and  $H_b = 4530$  m. For both values  $h = 270$  m,  $F_a$  is 72.3 and  $F_b$  75.6. Then, the velocity ( $v$ ) is estimated for both cases as:

$$v = 10 \cdot \sqrt{\frac{2 \cdot g \cdot h}{100 - F}} \quad (2)$$

where  $g$  is the acceleration of gravity ( $9.81 \text{ m s}^{-2}$ ). Thus, the obtained velocities are  $v_a = 138 \text{ m s}^{-1}$  and  $v_b = 147 \text{ m s}^{-1}$ . Compared to unconfined volcanic debris avalanches from the Andes (e.g. Parinacota, Socompa, and Lastarria), our minimum velocity estimates well in their range of 60–80  $\text{m s}^{-1}$  [Naranjo and Francis 1987; Clavero et al. 2002; Rodríguez et al. 2020]. On the other hand, the maximum velocities obtained here are comparable to those retrieved by the frictional model of Sosio et al. [2012]. A conservative mean velocity between these two end members is  $110 \text{ m s}^{-1}$ , comparable to the Antuco 7.1 ka debris avalanche ( $102 \text{ m s}^{-1}$ ), which became confined to the Laja River valley [Romero et al. 2022].

The large volume of the PTAD determined its extensive distribution in the central valley when becoming unconfined

(Figure 14B). Accordingly, the hummock density is higher toward the margins of the ring-plain deposit as observed in other VDADs [Siebert 1984]. We suggest that the PTAD behaves as a massive debris flow during deposition, accommodating large blocks in the flow direction, as demonstrated by hummock elongations in the central depression (Figures 4, 7F).

#### 7.5 Morphology and glacial erosion

Our observations of the pre-collapse components agree with glacial interaction as we identified large hackly-jointed lava blocks. In this regard, water derived from ice melting during lava emplacement can cause penetrative jointing, producing fragmental structures of between 10 and 20 cm, as well as the cooling of the groundmass [Gilbert et al. 1996; Lescinsky and Sisson 1998; Lescinsky and Fink 2000; Mee et al. 2009; Lachowycz et al. 2015]. Glacial interaction is also supported by the numerous lahars that cover the PTAD to the west (Figure 13B). Extensive ice coverage should have continued during the emplacement of the post-collapse Planchón lavas, as these show the same hackly-jointed features in the upper 40 % vertical sections. This implies that the pre- and post-collapse climate conditions and hence the glacial coverage were roughly identical. Remarkably, these lavas are only preserved in the northern margin of the Claro River valley, near Berta creek (Figure 2), suggesting they flowed laterally through the space left between the glacier and the valley slope. An analogous situation was observed during the 1991 lava of Hudson volcano [Naranjo 1993]. We propose that at c. 47 ka, the Claro River valley hosted a glacier that may have reached 0.6–1.0 km width, up to 70 m thick (contour line of 1030 m asl) and up to 19 km long to the WNW of the volcano. This evidence is also supported by the paleoclimatic reconstruction of Valero-Garcés et al. [2005], indicating a colder and moister climate than today in the Tagua Tagua site (100 km NW from Planchón) between 46 and 42 ky, thus allowing glacial advance in the Andes. In consequence, the role of ice retreat is again ruled out as an important condition to produce edifice instability.

#### 7.6 The further Holocene destruction of the Planchón volcano

According to Tormey [1989], the post-collapse Planchón was partially destroyed by glaciations and further explosive activity of “Peteroa” volcano, but that work does not provide a detailed description of the sequence of events that drove such edifice destruction. Further, Tormey [2010] argues that the largest proportion of pyroclastic deposits at the post-collapse Planchón may have favored rapid self-destruction of the cone by lahars and landslides. We expand this reasoning in the next few paragraphs. Post-collapse Planchón was built nested within the volcanic avalanche collapse caldera, with an elongated oval shape of  $2.0 \times 2.5$  km diameter, from which the northern and western margins are preserved (Figures 2, 3, and 13C). The current remnants of the collapse scar, obliterated by glacial erosion and the building of the post-collapse Planchón, suggest that the original collapse scar may have had a horse-shoe shape, breached to the west, and limited to the south by a cliff partially cutting the edifice of Azufre volcano (c. 230 m-

high). Since the colder climate prevailed until c. 12 ka BP, ice was retreating at about 7 ka BP (Figure 13D1).

The 7 ka BP activity began with a moderate explosive eruption (likely vigorous Strombolian to sub-Plinian), producing a complex, multiphase lithic-rich tephra fall deposit (Figure 13D2). Similar lithic-rich tephra have been associated with progressive cone truncation or vent erosion during the eruption (e.g. Mil Hojas unit at Puyehue-Cordón Caulle [Naranjo et al. 2017]).

Later, field evidence indicates that the Valenzuela diluted PDC deposit was emplaced with high energy to the east, northeast, and southeast (Figure 13D3). In contrast, on the western Planchon slope, only massive lahar deposits are distinguished but possibly associated with this eruption. The high lithic content within this deposit and its PDC characteristics indicates either widespread erosion in the feeding vents or the explosive fragmentation of the eastern avalanche caldera wall during the eruption. In addition, the VPDC deposit shows some key depositional features, such as palagonitic glass halos in the juvenile material, vesicles up to 4 mm trapped in fine ash layers 2 to 3 cm thick, ‘flame’-shaped load structures, and soft-sediment deformation inside the deposits, especially at medial distances (Figure 11). Mainly, palagonite formation has been observed in subglacial eruptions [e.g. Walker and Blake 1966], while loading and soft-sediment deformation structures are typical in dilute PDCs from phreatomagmatic eruptions [Smith and Kokelaar 2013; Douillet et al. 2015]. Considering the shape of the resulting crater and the erupted volume (c. 1.13 km<sup>3</sup>) of the VPDC, its parental eruption should have had characteristics resembling a small caldera-forming event. Given all these evidences, we propose that the VPDC can be classified as a lag breccia, forming a dilute PDC deposit of phreatomagmatic origin [e.g. Druitt 1985; Yamagata 1991]. The high content in lithics of these flows is also reflected in their distribution; their volume ( $V$ ) vs.  $A/V^{2/3}$  plot in the field of debris avalanches rather than in one of the pumice flows or block-and-ash flows (Figure 14C).

The last explosive event of this sequence is represented by the Los Ciegos laminar PDC deposit (Figure 13D4), which reached 0.012 km<sup>3</sup>. Its distribution parameters resemble that of pumice flows (Figure 14C). The dark appearance of the deposit surface due to a notorious enrichment of black cauliflower-shaped glassy bombs surrounded by a fine ash matrix are classically interpreted as a result of boiling-over eruptions emplacing hot PDCs [e.g. Rader et al. 2015]. Cauliflower bombs are frequent in phreatomagmatic PDCs [e.g. Lohmar et al. 2007], and their vesicularity decreases markedly from their core to rims due to rapid quenching. The ragged crust is frequent at the millimeter scale, typical of hydrovolcanic fragmentation processes [Fisher and Schmincke 1984].

## 7.7 Hazard implications

Previously, the work of Tormey [2010] envisaged a series of steps required to manage the risk of catastrophic glacio-volcanic events at the PPVC, namely 1) hazard characterization, 2) consequence characterization, 3) risk assessment, 4) risk control and countermeasures, and 4) risk communication.

Such considerations can be applied to further volcanoes with similar hazard condition. Considering the factors that contributed to Planchón’s instability, more research is encouraged in other volcanoes in the same critical condition, as is the case of Llaima, the most volumetric Southern Andes composite stratovolcano, with 380–400 km<sup>3</sup> [Naranjo and Moreno 2005; Völker et al. 2011]. The volcano hosts a 17 km-long fissure formed by numerous parasitic cones of <3 ky, which borders the western and northern flanks of the edifice. In addition, the most critical eruptions in recent centuries (AD 1640, 1751, 1945–1946, 1956–1957, 1994, 2007–2009) have shown a marked fissure style on the volcano’s flanks [Naranjo and Moreno 2005]. Furthermore, a 2500 m<sup>3</sup> zone of the highly oxidized northwest flank postdating the 1751 CE lava emission collapsed. Dungan et al. [2008] already suggested that assessing the modification of Llaima’s edifice is crucial, with the primary objective of evaluating its hazard. After the 2007–2009 eruptive cycle, Llaima experienced an 11 cm subsidence in its SE flank due to creeping and incipient collapse [Fournier et al. 2010]. Also, Franco et al. [2019] concluded that after this eruptive cycle, the summit area of Llaima increased its instability because of the abundant dykes intersecting the flanks and forming fractures and fissures. This highly recurrent active volcano presents a notably steep northern flank with 41 % (c. 25°) for the upper 1200 m, with a total slope close to 2100 m towards the Río Blanco valley, on the direct route to Curacautín (c. 20,000 inhabitants), 32 km NNW of the volcano [Naranjo and Moreno 2005]. A Planchón-type debris avalanche at Llaima volcano would have run out of c. 57 km, thus exceeding 25 km downstream of Curacautín. Consequently, it is highly recommended to integrate the collapse hazard of Llaima in future studies. Therefore, it is necessary to know the potential of edifice collapse, especially during an eruption, and its implications for ongoing civil protection decisions (e.g. the transitory meeting points for Curacautín [Vera et al. 2021]). To a certain extent, following the recommendations of Cassidy and Mani [2022], coordinated actions should be prioritized, assuming large-scale investments, to mitigate the effects of such scenarios.

Another potentially dangerous volcano is San José, with a 374 km<sup>3</sup> complex edifice [Völker et al. 2011]. San José is a basaltic-andesite volcanic complex that underwent mild phreatomagmatic eruptions in the 19th and 20th centuries [López-Escobar et al. 1985; Global Volcanism Program 2013] and lies 80 km SSE from Santiago de Chile. The existent volcanic hazard map considers the potential of a lateral collapse given its height > 3 km above an inclined base and steep flanks (27–35° [Silva Parejas and Orozco 2015]). A future debris avalanche of San José is not unlikely as its Pleistocene neighbor Mt. Marmolejo volcano produced a debris avalanche traveling 20 km west and descending 3.4 km from its source, only 2.4 ka BP [Thiele 1981; Melo et al. 2022]. Hence, we urge incorporating the potential collapse events in the hazard assessment and their related debris avalanche hazard zones.

Antuco, another basaltic SAVZ stratovolcano, also experienced a catastrophic lateral collapse during the Holocene experiencing a rapid post-collapse reconstruction [Romero et al. 2021; 2022; 2023], increasing its collapse potential.

## 8 CONCLUSIONS

Two major destructive events have affected the morphology of the Planchón volcano since the Late Pleistocene. The first consisted of a lateral collapse and destroyed the volcano's west flank at 48 ka BP, forming the Planchón-Teno debris avalanche confined to the Rio Claro River valley, which traveled up to c. 260 km h<sup>-1</sup> and reached 95 km to the west. The second was the multiphase Valenzuela explosive eruption that occurred at 7 ka BP, which destroyed the eastern remnants of the collapsed 48 ka BP amphitheater.

The Planchón-Teno debris avalanche deposit totalizes c. 8.6 ± 1.3 km<sup>3</sup> and is characterized by a hummocky surface; hummocks show an overall decrease of their volume with distance from the source, and their longer axes are orientated according to the flow direction. We suggest that the volcano was predisposed to collapse due to its rapid growth (0.30–0.48 km<sup>3</sup> ky<sup>-1</sup>) and the inclined geometry of the substratum (7° to 17° towards the west), which is also composed of soft lithologies (Jurassic sandstones, limestones, and conglomerates). Our textural analyses rule out hydrothermal alteration as a significant factor contributing to edifice instability.

The geochemistry of the pre-and post-collapse samples does not indicate any substantial change in the plumbing system because of the collapse, thus pointing to a monotonous mafic (i.e. basaltic andesite) behavior of the edifice. The ubiquitous hackly-jointed features in the post-collapse lavas demonstrate an extensive ice coverage that was likely emplaced in the margins of the valley filled by a paleo glacier at c. 47 ky BP. We suggest the long-term monotonous behavior and rapid growth of the Planchón volcano result from a complex structural network influenced by temporary crustal compression-relaxation cycles driving a steady supply of dense, mafic magma through these crustal damage zones.

Lately, the multiphase Valenzuela eruption formed an elongated oval shape (2.0 × 2.5 km-diameter) caldera, from which the products (1.12 km<sup>3</sup>) consist of lithic-rich tephra fall, lag breccia, and laminar PDCs also lithic-rich. The facies, componentry, and textural features of the deposit indicate a phreatomagmatic origin that was probably conditioned by magma-ice interactions.

Our reconstruction of these catastrophic events warns of the hazards of rapidly growing mafic volcanoes. It can be extrapolated to other similar edifices near their limit equilibrium, especially Llaima volcano.

## AUTHOR CONTRIBUTIONS

JAN funding acquisition, fieldwork on western and eastern flank and Google Earth photogeology mapping, formal analysis, manuscript design and writing. JER fieldwork, formal analysis, manuscript design and writing, elaboration of figures. JPC fieldwork, formal analysis, manuscript editing. YO formal analysis, manuscript editing. KS Distal facies fieldwork, manuscript editing. MJH eastward fieldwork, manuscript editing. HS formal unspiked K-Ar dating analysis.

## ACKNOWLEDGEMENTS

This work was initially supported by Fondecyt Project N° 1960186 and is a contribution to the Plan Nacional de Geología (PNG) of the Servicio Nacional de Geología y Minería (National Geology and Mining Survey), Chile (JAN and JPC). JER is financed through NSFGEONERC-funded project Dis-Eqm (NE/N018575/1), V-PLUS and the Dean's Award of the University of Manchester. We thank Dr. Lewis Hughes for handling and support with the Quanta 650 ESEM based at the Williamson Research Centre Mineral Analysis Facility. The authors are grateful with the insightful reviews of Dr. Pablo Forte and as well as an anonymous reviewer, in addition to the editorial handling by Dr. Engielle Paguican, that contributed to improve this manuscript.

## DATA AVAILABILITY

All data used in this report is available under request.

## COPYRIGHT NOTICE

© The Author(s) 2024. This article is distributed under the terms of the [Creative Commons Attribution 4.0 International License](https://creativecommons.org/licenses/by/4.0/), which permits unrestricted use, distribution, and reproduction in any medium, provided you give appropriate credit to the original author(s) and the source, provide a link to the Creative Commons license, and indicate if changes were made.

## REFERENCES

- Aguilera, F., Ó. Benavente, F. Gutiérrez, J. Romero, O. Saltori, R. González, M. R. Agosto, A. T. Caselli, and M. Pizarro (2016). "Eruptive activity of Planchón-Peteroa volcano for period 2010-2011, southern andean volcanic zone, Chile". *Andean Geology* 43 (1), pages 20–46.
- Baloga, S., P. D. Spudis, and J. E. Guest (1995). "The dynamics of rapidly emplaced terrestrial lava flows and implications for planetary volcanism". *Journal of Geophysical Research: Solid Earth* 100(B12), pages 24509–24519. DOI: [10.1029/95jb02844](https://doi.org/10.1029/95jb02844).
- Bonali, F. L., A. Tibaldi, C. Corazzato, D. R. Tormey, and L. E. Lara (2013). "Quantifying the effect of large earthquakes in promoting eruptions due to stress changes on magma pathway: The Chile case". *Tectonophysics* 583, pages 54–67. DOI: [10.1016/j.tecto.2012.10.025](https://doi.org/10.1016/j.tecto.2012.10.025).
- Carrasco, R. H. (2002). "Actividad eruptiva del complejo volcánico Planchón-Peteroa-Azufre". *Boletín de Geografía* (16), pages 97–122.
- Cassidy, M. and L. Mani (2022). "Huge volcanic eruptions: time to prepare". *Nature* 608(7923), pages 469–471. DOI: [10.1038/d41586-022-02177-x](https://doi.org/10.1038/d41586-022-02177-x).
- Charrier, R., O. Baeza, S. Elgueta, J. Flynn, P. Gans, S. Kay, N. Muñoz, A. Wyss, and E. Zurita (2002). "Evidence for Cenozoic extensional basin development and tectonic inversion south of the flat-slab segment, southern Central Andes, Chile (33°–36°S.L.)". *Journal of South American Earth Sciences* 15(1), pages 117–139. DOI: [10.1016/s0895-9811\(02\)00009-3](https://doi.org/10.1016/s0895-9811(02)00009-3).

- Charrier, R., L. Iturrizaga, S. Carretier, and V. Regard (2019). “Geomorphologic and Glacial Evolution of the Cachapoal and southern Maipo catchments in the Andean Principal Cordillera, Central Chile (34°–35° S)”. *Andean Geology* 46(2), page 240. DOI: [10.5027/andgeov46n2-3108](https://doi.org/10.5027/andgeov46n2-3108).
- Charrier, R., A. Wyss, J. Flynn, C. Swisher III, S. Spichiger, and F. Zapatta (1994). “Nuevos antecedentes estratigráficos y estructurales para las Formaciones Coya-Machalí y Abanico, entre 33° 50' y 35° S, Cordillera Principal Chilena”. *Congreso Geológico Chileno*. Volume 7, pages 1316–1319.
- Clavero, J., R. Sparks, H. Huppert, and W. Dade (2002). “Geological constraints on the emplacement mechanism of the Parinacota debris avalanche, northern Chile”. *Bulletin of Volcanology* 64(1), pages 40–54. DOI: [10.1007/s00445-001-0183-0](https://doi.org/10.1007/s00445-001-0183-0).
- Comte, D., M. Farías, R. Charrier, and A. González (2008). “Active tectonics in the Central Chilean Andes: 3D tomography based on the aftershock sequence of the 28 August 2004 shallow crustal earthquake”. *International Symposium on Andean Geodynamics (ISAG 2008, Nice)*. Volume 7, pages 160–163.
- Davidson, J. and J. C. Vicente (1973). “Características paleogeográficas y estructurales del área fronteriza de las nacientes del Teno (Chile) y Santa Elena (Argentina)(Cordillera Principal, 35 a 35 15'latitud sur)”. *Congreso Geológico Argentino*. 5, pages 11–55.
- Douillet, G. A., B. Taisne, È. Tsang-Hin-Sun, S. K. Müller, U. Kueppers, and D. B. Dingwell (2015). “Syn-eruptive, soft-sediment deformation of deposits from dilute pyroclastic density current: triggers from granular shear, dynamic pore pressure, ballistic impacts and shock waves”. *Solid Earth* 6(2), pages 553–572. DOI: [10.5194/se-6-553-2015](https://doi.org/10.5194/se-6-553-2015).
- Druitt, T. H. (1985). “Vent Evolution and Lag Breccia Formation during the Cape Riva Eruption of Santorini, Greece”. *The Journal of Geology* 93(4), pages 439–454. DOI: [10.1086/628965](https://doi.org/10.1086/628965).
- Dufresne, A., S. Salinas, and C. Siebe (2010). “Substrate deformation associated with the Jocotitlán edifice collapse and debris avalanche deposit, Central México”. *Journal of Volcanology and Geothermal Research* 197(1–4), pages 133–148. DOI: [10.1016/j.jvolgeores.2010.02.019](https://doi.org/10.1016/j.jvolgeores.2010.02.019).
- Dungan, M., C. Bouvet de Maisonneuve, D. Sellés, J. A. Naranjo, H. Moreno, C. Langmuir, O. Reubi, S. Goldstein, J. Jweda, S. Escrig, et al. (2008). “Volcán Llaima (38.7° S, Chilean Southern Volcanic Zone): insights into a dominantly mafic and ‘hyperactive’ subduction-related magmatic system”. *International Symposium on Andean Geodynamics (ISAG 2008, Nice)*. Volume 7.
- Elsworth, D. and S. J. Day (1999). “Flank collapse triggered by intrusion: the Canarian and Cape Verde Archipelagoes”. *Journal of Volcanology and Geothermal Research* 94(1–4), pages 323–340. DOI: [10.1016/s0377-0273\(99\)00110-9](https://doi.org/10.1016/s0377-0273(99)00110-9).
- Elsworth, D. and B. Voight (1996). “Evaluation of volcano flank instability triggered by dyke intrusion”. *Geological Society, London, Special Publications* 110(1), pages 45–53. DOI: [10.1144/gsl.sp.1996.110.01.03](https://doi.org/10.1144/gsl.sp.1996.110.01.03).
- Espizua, L. E. (2000). “Variaciones glaciarias del Holoceno en el valle del río Valenzuela, Mendoza”. *XII Reunión de Campo del Cuaternario, Comité Argentino para la Investigación del Cuaternario (CADINCUA). Resúmenes y Guía de Campo*, page 6.
- Farías, M., D. Comte, R. Charrier, J. Martinod, C. David, A. Tassara, F. Tapia, and A. Fock (2010). “Crustal-scale structural architecture in central Chile based on seismicity and surface geology: Implications for Andean mountain building”. *Tectonics* 29(3). DOI: [10.1029/2009tc002480](https://doi.org/10.1029/2009tc002480).
- Fisher, R. V. and H.-U. Schmincke (1984). “Pyroclastic Flow Deposits”. *Pyroclastic Rocks*. Springer Berlin Heidelberg, pages 186–230. ISBN: 9783642748646. DOI: [10.1007/978-3-642-74864-6\\_8](https://doi.org/10.1007/978-3-642-74864-6_8).
- Fleck, R. J., J. F. Sutter, and D. H. Elliot (1977). “Interpretation of discordant 40Ar/39Ar age-spectra of mesozoic tholeiites from antarctica”. *Geochimica et Cosmochimica Acta* 41(1), pages 15–32. DOI: [10.1016/0016-7037\(77\)90184-3](https://doi.org/10.1016/0016-7037(77)90184-3).
- Flynn, J. J., A. R. Wyss, R. Charrier, and C. C. Swisher (1995). “An Early Miocene anthropoid skull from the Chilean Andes”. *Nature* 375(6528), pages 253–253. DOI: [10.1038/375253c0](https://doi.org/10.1038/375253c0).
- Fock, A., R. Charrier, V. MaksaeV, and M. Farías (2006). “Neogene exhumation and uplift of the Andean Main Cordillera from apatite fission tracks between 33°30' and 34°00'S”. *Backbone of the Americas—Patagonia to Alaska. Geological Society of America Meeting, Mendoza*. Volume 102.
- Fournier, T. J., M. E. Pritchard, and S. N. Riddick (2010). “Duration, magnitude, and frequency of subaerial volcano deformation events: New results from Latin America using InSAR and a global synthesis”. *Geochemistry, Geophysics, Geosystems* 11(1). DOI: [10.1029/2009gc002558](https://doi.org/10.1029/2009gc002558).
- Francis, P. W. and M. C. W. Baker (1977). “Mobility of pyroclastic flows”. *Nature* 270(5633), pages 164–165. DOI: [10.1038/270164a0](https://doi.org/10.1038/270164a0).
- Franco, L., J. L. Palma, L. E. Lara, F. Gil-Cruz, C. Cardona, D. Basualto, and J. San Martín (2019). “Eruptive sequence and seismic activity of Llaima volcano (Chile) during the 2007–2009 eruptive period: Inferences of the magmatic feeding system”. *Journal of Volcanology and Geothermal Research* 379, pages 90–105. DOI: [10.1016/j.jvolgeores.2019.04.014](https://doi.org/10.1016/j.jvolgeores.2019.04.014).
- Gilbert, J. S., M. V. Stasiuk, S. J. Lane, C. R. Adam, M. D. Murphy, R. S. J. Sparks, and J. A. Naranjo (1996). “Non-explosive, constructional evolution of the ice-filled caldera at Volcán Sollipulli, Chile”. *Bulletin of Volcanology* 58(1), pages 67–83. DOI: [10.1007/s004450050127](https://doi.org/10.1007/s004450050127).
- Gillot, P. Y., S. Chiesa, G. Pasquare, and L. Vezzoli (1982). “< 33,000-yr K–Ar dating of the volcano–tectonic horst of the Isle of Ischia, Gulf of Naples”. *Nature* 299(5880), pages 242–245.
- Glicken, H. (1991). “Sedimentary architecture of large volcanic-debris avalanches”. *Sedimentation in Volcanic Settings*. SEPM (Society for Sedimentary Geology), pages 99–106. DOI: [10.2110/pec.91.45.0099](https://doi.org/10.2110/pec.91.45.0099).
- Global Volcanism Program (2013). “San Jose (357020)”. *Volcanoes of the World, v. 4.11.0*. Edited by E. Venzke. Smithsonian Institution. [online].
- González Ferrán, O. (1995). *Volcanes de Chile*. Instituto Geográfico Militar.

- Goto, Y., T. Danhara, and A. Tomiya (2019). “Catastrophic sector collapse at Usu volcano, Hokkaido, Japan: failure of a young edifice built on soft substratum”. *Bulletin of Volcanology* 81(6). DOI: [10.1007/s00445-019-1293-x](https://doi.org/10.1007/s00445-019-1293-x).
- Grosse, P., Y. Orihashi, S. R. Guzmán, H. Sumino, and K. Nagao (2018). “Eruptive history of Incahuasi, Falso Azufre and El Cónдор Quaternary composite volcanoes, southern Central Andes”. *Bulletin of Volcanology* 80(5). DOI: [10.1007/s00445-018-1221-5](https://doi.org/10.1007/s00445-018-1221-5).
- Guillou, H., B. Van Vliet-Lanoë, A. Guðmundsson, and S. Nomade (2010). “New unspiked K–Ar ages of Quaternary subglacial and sub-aerial volcanic activity in Iceland”. *Quaternary Geochronology* 5(1), pages 10–19. DOI: [10.1016/j.quageo.2009.08.007](https://doi.org/10.1016/j.quageo.2009.08.007).
- Haller, M. J., J. E. Mendía, and H. A. Oстера (1991). “Mapa preliminar de riesgo en la vertiente Argentina del volcán Peteroa”. *Congreso Geológico Chileno Actas*. Volume 6. Santiago, pages 355–358.
- Haller, M. J., H. A. Oстера, A. H. Pesce, M. Gardini, and A. Folguera (1994). “Vulcanoestratigrafía reciente y eruptividad del volcán Peteroa”. *Congreso Geológico Chileno Actas*. Volume 7. Actas, pages 319–323.
- Haller, M. J. and C. Risso (2011). “La erupción del volcán Peteroa (35°15'S, 70°18'O) del 4 de septiembre de 2010”. *Revista de la Asociación Geológica Argentina* 68(2), pages 295–305.
- Hauser, A. (1990). *Carta hidrogeológica de Chile: hoja Rancagua VI región*. Volume 1. Servicio Nacional de Geología y Minería.
- (1993). *Remociones en mas en Chile*. 45. Servicio Nacional de Geología y Minería.
- Hildreth, W., B. Singer, E. Godoy, and F. Munizaga (1998). “The age and constitution of Cerro Campanario, a mafic stratovolcano in the Andes of Central Chile”. *Revista geológica de Chile* 25(1). DOI: [10.4067/s0716-02081998000100002](https://doi.org/10.4067/s0716-02081998000100002).
- Holbik, S. P. (2014). “Arc Crust-Magma Interaction in the Andean Southern Volcanic Zone from Thermobarometry, Mineral Composition, Radiogenic Isotope and Rare Earth Element Systematics of the Azufre-Planchon-Peteroa Volcanic Complex, Chile”. PhD thesis. Florida International University.
- Jara-Muñoz, J., D. Melnick, P. Zambrano, A. Rietbrock, J. González, B. Argandoña, and M. R. Strecker (2017). “Quantifying offshore fore-arc deformation and splay-fault slip using drowned Pleistocene shorelines, Arauco Bay, Chile”. *Journal of Geophysical Research: Solid Earth* 122(6), pages 4529–4558. DOI: [10.1002/2016jb013339](https://doi.org/10.1002/2016jb013339).
- Keigler, R., J.-C. Thouret, K. A. Hodgson, V. E. Neall, J. A. Lecointre, J. N. Procter, and S. J. Cronin (2011). “The Whangaehu Formation: Debris-avalanche and lahar deposits from ancestral Ruapehu volcano, New Zealand”. *Geomorphology* 133(1–2), pages 57–79. DOI: [10.1016/j.geomorph.2011.06.019](https://doi.org/10.1016/j.geomorph.2011.06.019).
- Klug, J. D., A. Ramirez, B. S. Singer, B. R. Jicha, E. E. Mixon, and P. Martinez (2022). “Intercalibration of the Servicio Nacional de Geología y Minería (SERNAGEOMIN), Chile and WiscAr 40Ar/39Ar laboratories for Quaternary dating”. *Quaternary Geochronology* 72, page 101354. DOI: [10.1016/j.quageo.2022.101354](https://doi.org/10.1016/j.quageo.2022.101354).
- Lachowycz, S. M., D. M. Pyle, J. S. Gilbert, T. A. Mather, K. Mee, J. A. Naranjo, and L. K. Hobbs (2015). “Glaciovolcanism at Volcán Sollipulli, southern Chile: Lithofacies analysis and interpretation”. *Journal of Volcanology and Geothermal Research* 303, pages 59–78. DOI: [10.1016/j.jvolgeores.2015.06.021](https://doi.org/10.1016/j.jvolgeores.2015.06.021).
- Le Maitre, R. W., A. Streckeisen, B. Zanettin, M. J. Le Bas, B. Bonin, and P. Bateman (2002). *Igneous Rocks: A Classification and Glossary of Terms*. Cambridge University Press. ISBN: 9780511535581. DOI: [10.1017/cbo9780511535581](https://doi.org/10.1017/cbo9780511535581).
- Lescinsky, D. T. and T. W. Sisson (1998). “Ridge-forming, ice-bounded lava flows at Mount Rainier, Washington”. *Geology* 26(4), page 351. DOI: [10.1130/0091-7613\(1998\)026<0351:rflbf>2.3.co;2](https://doi.org/10.1130/0091-7613(1998)026<0351:rflbf>2.3.co;2).
- Lescinsky, D. T. and J. H. Fink (2000). “Lava and ice interaction at stratovolcanoes: Use of characteristic features to determine past glacial extents and future volcanic hazards”. *Journal of Geophysical Research: Solid Earth* 105(B10), pages 23711–23726. DOI: [10.1029/2000jb900214](https://doi.org/10.1029/2000jb900214).
- Leyrit, H. (2000). “Flank collapse and debris avalanche deposits”. *Volcanics rocks from magma to sediments*. Edited by H. Leyrit and C. Montenat. CRC Press, Amsterdam, pages 111–129.
- Lohmar, S., C. Robin, A. Gourgaud, J. Clavero, M. Á. Parada, H. Moreno, O. Ersoy, L. López-Escobar, and J. A. Naranjo (2007). “Evidencias de interacción magma-agua durante el ciclo eruptivo explosivo de la Ignimbrita Licán (13.800 años AP), volcán Villarrica (sur de Chile)”. *Revista geológica de Chile* 34(2), pages 233–247. DOI: [10.4067/S0716-02082007000200004](https://doi.org/10.4067/S0716-02082007000200004).
- López-Escobar, L., H. Moreno, M. Tagiri, K. Notsu, and N. Onuma (1985). “Geochemistry and petrology of lavas from San Jose volcano, Southern Andes (33.3°S).” *Geochemical Journal* 19(4), pages 209–222. DOI: [10.2343/geochemj.19.209](https://doi.org/10.2343/geochemj.19.209).
- MacPhail, D. D. (1973). “The Geomorphology of the Rio Teno Lahar, Central Chile”. *Geographical Review* 63(4), page 517. DOI: [10.2307/213919](https://doi.org/10.2307/213919).
- Mathieu, L., B. van Wyk de Vries, M. Pilato, and V. R. Troll (2011). “The interaction between volcanoes and strike-slip, transtensional and transpressional fault zones: Analogue models and natural examples”. *Journal of Structural Geology* 33(5), pages 898–906. DOI: [10.1016/j.jsg.2011.03.003](https://doi.org/10.1016/j.jsg.2011.03.003).
- McLeod, O. E. and A. Pittari (2021). “A channelized debris-avalanche deposit from Pirongia basaltic stratovolcano, New Zealand”. *Geological Society, London, Special Publications* 520(1), pages 191–209. DOI: [10.1144/sp520-2020-222](https://doi.org/10.1144/sp520-2020-222).
- Mee, K., J. S. Gilbert, D. W. McGarvie, J. A. Naranjo, and M. S. Pringle (2009). “Palaeoenvironment reconstruction, volcanic evolution and geochronology of the Cerro Blanco subcomplex, Nevados de Chillán volcanic complex, central Chile”. *Bulletin of Volcanology* 71(8), pages 933–952. DOI: [10.1007/s00445-009-0277-7](https://doi.org/10.1007/s00445-009-0277-7).

- Melo, V., G. Easton, and S. Rebolledo (2022). “On the genesis of a massive Holocene rock avalanche deposit in the Yeso River catchment, Andes Cordillera of central Chile”. *Geomorphology* 406, page 108214. DOI: [10.1016/j.geomorph.2022.108214](https://doi.org/10.1016/j.geomorph.2022.108214).
- Mileti, D. P. B., G. Fernandez, and R. Updike (1991). *The eruption of Nevado Del Ruiz Volcano Colombia, South America, November 13, 1985*. Volume 4. Committee on Natural Disasters, National Research Council, National Academy Press, Washington, D.C.
- Mixon, E. E., B. S. Singer, B. R. Jicha, and A. Ramirez (2021). “Calbuco, a monotonous andesitic high-flux volcano in the Southern Andes, Chile”. *Journal of Volcanology and Geothermal Research* 416, page 107279. DOI: [10.1016/j.jvolgeores.2021.107279](https://doi.org/10.1016/j.jvolgeores.2021.107279).
- Mosolf, J. G., P. B. Gans, A. R. Wyss, J. M. Cottle, and J. J. Flynn (2019). “Late Cretaceous to Miocene volcanism, sedimentation, and upper-crustal faulting and folding in the Principal Cordillera, central Chile: Field and geochronological evidence for protracted arc volcanism and transpressive deformation”. *GSA Bulletin*. DOI: [10.1130/b31998.1](https://doi.org/10.1130/b31998.1).
- Nagao, K., A. Ogata, Y. Miura, J.-i. Matsuda, and S.-i. Akimoto (1991). “Highly reproducible 13 and 17ka K-Ar ages of two volcanic rocks.” *Geochemical Journal* 25(6), pages 447–451. DOI: [10.2343/geochemj.25.447](https://doi.org/10.2343/geochemj.25.447).
- Naranjo, J. A. (1993). “La erupción del volcán Hudson en 1991 (46 S), Región XI, Aisen, Chile.” *Servicio Nacional de Geología y Minería Boletín* 44, pages 1–50.
- (2012). “Principales etapas evolutivas holocenas del volcán Planchón y su reactivación relacionada al megasismo del 27 de Febrero de 2010”. *Congreso Geológico Chileno*. 13, pages 440–441.
- Naranjo, J. A. and P. Francis (1987). “High velocity debris avalanche at Lastarria volcano in the north Chilean Andes”. *Bulletin of Volcanology* 49(2), pages 509–514. DOI: [10.1007/bf01245476](https://doi.org/10.1007/bf01245476).
- Naranjo, J. A. and M. J. Haller (2002). “Erupciones holocenas principalmente explosivas del volcán Planchón, Andes del sur (35°15'S)”. *Revista geológica de Chile* 29(1). DOI: [10.4067/s0716-02082002000100006](https://doi.org/10.4067/s0716-02082002000100006).
- Naranjo, J. A., M. J. F. Haller, H. A. Ostera, A. H. Pesce, and P. Sruoga (1999). “Geología y Peligros del Complejo Volcánico Planchón-Peteroa, Andes del Sur (35°15 S), Región del Maule, Chile-Provincia de Mendoza, Argentina”. *Servicio Nacional de Geología y Minería, Boletín* 52, page 55.
- Naranjo, J. A. and H. Moreno (2005). “Geología del volcán Llaima, región de La Araucanía, escala: 1: 50.000”.
- Naranjo, J. A., K. Scott, and W. Hildreth (1997). “Highly mobile catastrophic debris avalanche of Planchón-Peteroa volcanic complex, southern Andes, Central Chile”. *IAVCEI General Assembly, Abstracts*. Puerto Vallarta, page 107.
- Naranjo, J. A., B. S. Singer, B. R. Jicha, H. Moreno, and L. E. Lara (2017). “Holocene tephra succession of Pugehue-Cordón Caulle and Antillanca/Casablanca volcanic complexes, southern Andes (40–41°S)”. *Journal of Volcanology and Geothermal Research* 332, pages 109–128. DOI: [10.1016/j.jvolgeores.2016.11.017](https://doi.org/10.1016/j.jvolgeores.2016.11.017).
- Naranjo, J. A., V. Villa, C. Ramírez, and C. Pérez de Arce (2018). “Volcanism and tectonism in the southern Central Andes: Tempo, styles, and relationships”. *Geosphere* 14(2), pages 626–641. DOI: [10.1130/ges01350.1](https://doi.org/10.1130/ges01350.1).
- Naranjo, J. A. and D. Welkner (2004). “Informe sobre efectos del sismo del 28 de agosto 2004 en las nacientes del río Teno, VII Región”. *Servicio Nacional de Geología y Minería*.
- Orihashi, Y. and T. Hirata (2003). “Rapid quantitative analysis of Y and REE abundances in XRF glass bead for selected GSJ reference rock standards using Nd-YAG 266nm UV laser ablation ICP-MS.” *Geochemical Journal* 37(3), pages 401–412. DOI: [10.2343/geochemj.37.401](https://doi.org/10.2343/geochemj.37.401).
- Orihashi, Y., J. A. Naranjo, A. Motoki, H. Sumino, D. Hirata, R. Anma, and K. Nagao (2004). “Quaternary volcanic activity of Hudson and Lautaro volcanoes, Chilean Patagonia: New constraints from K-Ar ages”. *Revista geológica de Chile* 31(2). DOI: [10.4067/s0716-02082004000200002](https://doi.org/10.4067/s0716-02082004000200002).
- Paguican, E. M. R., B. van Wyk de Vries, and A. M. F. Lagmay (2014). “Hummocks: how they form and how they evolve in landslide-debris avalanches”. *Landslides* 11(1), pages 67–80. DOI: [10.1007/s10346-012-0368-y](https://doi.org/10.1007/s10346-012-0368-y).
- Pearce, R. K., A. Sánchez de la Muela, M. Moorkamp, J. O. S. Hammond, T. M. Mitchell, J. Cembrano, J. Araya Vargas, P. G. Meredith, P. Iturrieta, N. Pérez-Estay, N. R. Marshall, J. Smith, G. Yáñez, W. Ashley Griffith, C. Marquardt, A. Stanton-Yonge, and R. Núñez (2020). “Reactivation of Fault Systems by Compartmentalized Hydrothermal Fluids in the Southern Andes Revealed by Magnetotelluric and Seismic Data”. *Tectonics* 39(12). DOI: [10.1029/2019tc005997](https://doi.org/10.1029/2019tc005997).
- Peccerillo, A. and S. R. Taylor (1976). “Geochemistry of eocene calc-alkaline volcanic rocks from the Kastamonu area, Northern Turkey”. *Contributions to Mineralogy and Petrology* 58(1), pages 63–81. DOI: [10.1007/bf00384745](https://doi.org/10.1007/bf00384745).
- Pérez de Arce, C., S. Matthews, and J. Klein (2003). “Geochronology by the <sup>40</sup>Ar/<sup>39</sup>Ar method at the SERNA-GEOMIN Laboratory, Santiago, Chile”. *International Conference on Research Reactor, Utilization, Safety, Decommissioning, Fuel and Waste Management, Actas, Santiago*, pages 82–83.
- Perinotto, H., J.-L. Schneider, P. Bachèlery, F.-X. Le Bourdonnec, V. Famin, and L. Michon (2015). “The extreme mobility of debris avalanches: A new model of transport mechanism”. *Journal of Geophysical Research: Solid Earth* 120(12), pages 8110–8119. DOI: [10.1002/2015jb011994](https://doi.org/10.1002/2015jb011994).
- Pierson, T. C., R. J. Janda, J.-C. Thouret, and C. A. Borrero (1990). “Perturbation and melting of snow and ice by the 13 November 1985 eruption of Nevado del Ruiz, Colombia, and consequent mobilization, flow and deposition of lahars”. *Journal of Volcanology and Geothermal Research* 41(1–4), pages 17–66. DOI: [10.1016/0377-0273\(90\)90082-q](https://doi.org/10.1016/0377-0273(90)90082-q).
- Piquer, J., J. C. Castelli, R. Charrier, and G. Yáñez (2010). “El Cenozoico del alto río Teno, Cordillera Principal, Chile central: estratigrafía, plutonismo y su relación con estructuras profundas”. *Andean geology* 37(1). DOI: [10.4067/s0718-71062010000100002](https://doi.org/10.4067/s0718-71062010000100002).

- Piquer, J., G. Yáñez, O. Rivera, and D. R. Cooke (2019). “Long-lived crustal damage zones associated with fault intersections in the high Andes of Central Chile”. *Andean Geology* 46(2), pages 223–239. DOI: [10.5027/andgeoV46n2-3106](https://doi.org/10.5027/andgeoV46n2-3106).
- Ponomareva, V. V., I. V. Melekestsev, and O. V. Dirksen (2006). “Sector collapses and large landslides on Late Pleistocene–Holocene volcanoes in Kamchatka, Russia”. *Journal of Volcanology and Geothermal Research* 158(1–2), pages 117–138. DOI: [10.1016/j.jvolgeores.2006.04.016](https://doi.org/10.1016/j.jvolgeores.2006.04.016).
- Potere, D. (2008). “Horizontal Positional Accuracy of Google Earth’s High-Resolution Imagery Archive”. *Sensors* 8(12), pages 7973–7981. DOI: [10.3390/s8127973](https://doi.org/10.3390/s8127973).
- Pritchard, M. E., J. A. Jay, F. Aron, S. T. Henderson, and L. E. Lara (2013). “Subsidence at southern Andes volcanoes induced by the 2010 Maule, Chile earthquake”. *Nature Geoscience* 6(8), pages 632–636. DOI: [10.1038/ngeo1855](https://doi.org/10.1038/ngeo1855).
- Rader, E., D. Geist, J. Geissman, J. Dufek, and K. Harpp (2015). “Hot clasts and cold blasts: thermal heterogeneity in boiling-over pyroclastic density currents”. *Geological Society, London, Special Publications* 396(1), pages 67–86. DOI: [10.1144/sp396.16](https://doi.org/10.1144/sp396.16).
- Renne, P. R., A. L. Deino, R. C. Walter, B. D. Turrin, C. C. Swisher III, T. A. Becker, G. H. Curtis, W. D. Sharp, and A.-R. Jaouni (1994). “Intercalibration of astronomical and radioisotopic time”. *Geology* 22(9), page 783. DOI: [10.1130/0091-7613\(1994\)022<0783:ioart>2.3.co;2](https://doi.org/10.1130/0091-7613(1994)022<0783:ioart>2.3.co;2).
- Rodríguez, I., J. Páez, M. S. van Wyk de Vries, B. van Wyk de Vries, and B. Godoy (2020). “Dynamics and physical parameters of the Lastarria debris avalanche, Central Andes”. *Journal of Volcanology and Geothermal Research* 402, page 106990. DOI: [10.1016/j.jvolgeores.2020.106990](https://doi.org/10.1016/j.jvolgeores.2020.106990).
- Romagnoli, C., D. Casalbore, F. L. Chiocci, and A. Bosman (2009). “Offshore evidence of large-scale lateral collapses on the eastern flank of Stromboli, Italy, due to structurally-controlled, bilateral flank instability”. *Marine Geology* 262(1–4), pages 1–13. DOI: [10.1016/j.margeo.2009.02.004](https://doi.org/10.1016/j.margeo.2009.02.004).
- Romero, J. E., F. Aguilera, F. Delgado, D. Guzmán, A. R. Van Eaton, N. Luengo, J. Caro, J. Bustillos, A. Guevara, S. Holbik, D. R. Tormey, and I. Zegarra (2020). “Combining ash analyses with remote sensing to identify juvenile magma involvement and fragmentation mechanisms during the 2018/19 small eruption of Peteroa volcano (Southern Andes)”. *Journal of Volcanology and Geothermal Research* 402, page 106984. DOI: [10.1016/j.jvolgeores.2020.106984](https://doi.org/10.1016/j.jvolgeores.2020.106984).
- Romero, J. E., H. Moreno, M. Polacci, M. Burton, and D. Guzmán (2022). “Mid-Holocene lateral collapse of Antuco volcano (Chile): debris avalanche deposit features, emplacement dynamics, and impacts”. *Landslides* 19(6), pages 1321–1338. DOI: [10.1007/s10346-022-01865-z](https://doi.org/10.1007/s10346-022-01865-z).
- Romero, J. E., M. Polacci, F. Arzilli, C. I. Schipper, G. La Spina, M. Burton, M. A. Parada, J. Norambuena, A. Guevara, S. Watt, H. Moreno, L. Franco, and J. Fellowes (2023). “Long-term volcano evolution controlled by lateral collapse at Antuco volcano, southern Andes, Chile”. *Communications Earth & Environment* 4(1). DOI: [10.1038/s43247-023-00931-1](https://doi.org/10.1038/s43247-023-00931-1).
- Romero, J. E., M. Polacci, S. Watt, S. Kitamura, D. R. Tormey, G. Sielfeld, F. Arzilli, G. La Spina, L. Franco, M. Burton, and E. Polanco (2021). “Volcanic Lateral Collapse Processes in Mafic Arc Edifices: A Review of Their Driving Processes, Types and Consequences”. *Frontiers in Earth Science* 9. DOI: [10.3389/feart.2021.639825](https://doi.org/10.3389/feart.2021.639825).
- Rossel, P., V. Oliveros, J. Mescua, F. Tapia, M. N. Ducea, S. Calderón, R. Charrier, and D. Hoffman (2014). “The Upper Jurassic volcanism of the Rio Damas-Tordillo Formation (33–35.5 S): Insights on petrogenesis, chronology, provenance and tectonic implications”. *Andean Geology* 41(3), pages 529–557. DOI: [10.5027/andgeoV41n3-a03](https://doi.org/10.5027/andgeoV41n3-a03).
- Roverato, M., P. Larrea, I. Casado, M. Mulas, G. Béjar, and L. Bowman (2018). “Characterization of the Cubilche debris avalanche deposit, a controversial case from the northern Andes, Ecuador”. *Journal of Volcanology and Geothermal Research* 360, pages 22–35. DOI: [10.1016/j.jvolgeores.2018.07.006](https://doi.org/10.1016/j.jvolgeores.2018.07.006).
- Ruiz, S. and R. Madariaga (2018). “Historical and recent large megathrust earthquakes in Chile”. *Tectonophysics* 733, pages 37–56. DOI: [10.1016/j.tecto.2018.01.015](https://doi.org/10.1016/j.tecto.2018.01.015).
- Scott, K. M., J. L. Macias, J. W. Vallance, J. A. Naranjo, S. Rodríguez, and J. P. McGeehin (2001). “Catastrophic debris flows transformed from landslides in volcanic terrains: mobility, hazard assessment, and mitigation strategies”. (1630). U.S. Geological Survey Professional Paper 1630.
- Servicio Nacional de Geología y Minería (SERNAGEOMIN) (2010). “Reporte Especial de Actividad Volcánica No. 4, Región del Maule, Grupo Volcánico Planchón-Peteroa, 10 de septiembre de 2010, 20 hrs”. *Servicio Nacional de Geología y Minería*.
- Sharma, A. and D. Gupta (2014). “Derivation of topographic map from elevation data available in google earth”. *Civil Engineering and Urban Planning* 1(2), pages 14–21.
- Siebert, L. (1984). “Large volcanic debris avalanches: Characteristics of source areas, deposits, and associated eruptions”. *Journal of Volcanology and Geothermal Research* 22(3–4), pages 163–197. DOI: [10.1016/0377-0273\(84\)90002-7](https://doi.org/10.1016/0377-0273(84)90002-7).
- Siebert, L., H. Glicken, and T. Ui (1987). “Volcanic hazards from Bezymianny- and Bandai-type eruptions”. *Bulletin of Volcanology* 49(1), pages 435–459. DOI: [10.1007/bf01046635](https://doi.org/10.1007/bf01046635).
- Silva Parejas, C. and G. Orozco (2015). “Peligros del Complejo Volcánico San José, Cajón del Maipo, Región Metropolitana de Santiago, Chile.” *Congreso Geológico Chileno Actas*. Volume 15. La Serena, pages 37–40.
- Smith, N. J. and B. P. Kokelaar (2013). “Proximal record of the 273 ka Poris caldera-forming eruption, Las Cañadas, Tenerife”. *Bulletin of Volcanology* 75(11). DOI: [10.1007/s00445-013-0768-4](https://doi.org/10.1007/s00445-013-0768-4).
- Sosio, R., G. B. Crosta, and O. Hungr (2012). “Numerical modeling of debris avalanche propagation from collapse of volcanic edifices”. *Landslides* 9(3), pages 315–334. DOI: [10.1007/s10346-011-0302-8](https://doi.org/10.1007/s10346-011-0302-8).
- Stern, C. R. (2004). “Active Andean volcanism: its geologic and tectonic setting”. *Revista geológica de Chile* 31(2). DOI: [10.4067/s0716-02082004000200001](https://doi.org/10.4067/s0716-02082004000200001).

- Stern, C. R., H. Moreno, L. López-Escobar, J. E. Clavero, L. E. Lara, J. A. Naranjo, M. A. Parada, and M. A. Skewes (no date). “Chilean volcanoes”. *The Geology of Chile*. Edited by T. Moreno and W. Gibbons. The Geological Society of London, pages 147–178. ISBN: 9781862392205. DOI: [10.1144/goch.5](https://doi.org/10.1144/goch.5).
- Sun, S.-s. and W. F. McDonough (1989). “Chemical and isotopic systematics of oceanic basalts: implications for mantle composition and processes”. *Geological Society, London, Special Publications* 42(1), pages 313–345. DOI: [10.1144/gsl.sp.1989.042.01.19](https://doi.org/10.1144/gsl.sp.1989.042.01.19).
- Tani, K., Y. Orihashi, and S. Nakada (2002). “Major and trace components analysis of silicate rocks by X-ray fluorescence spectrometer using fused glass beads: evaluation of analytical precision of three, six, eleven times dilution fused glass beads methods”. *Technical Research Report, Earthquake Research Institute, University of Tokyo* 8, pages 26–36.
- Thiele, R. (1981). “Carta Geológica de Chile, Escala 1: 250.000, Hoja de Santiago, Region Metropolitana”. *Instituto de Investigaciones Geológicas, Cartas* (39). [Map].
- Tibaldi, A., F. Pasquarè, and D. R. Tormey (2010). “Volcanism in Reverse and Strike-Slip Fault Settings”. *New Frontiers in Integrated Solid Earth Sciences*. Edited by S. Cloetingh and J. Negendank. Springer Netherlands, pages 315–348. ISBN: 9789048127375. DOI: [10.1007/978-90-481-2737-5\\_9](https://doi.org/10.1007/978-90-481-2737-5_9).
- Tormey, D. R. (1989). “Geology and geochemistry of the active Azufre-Planchon-Peteroa volcanic center (3515’S, southern Andes): implications for Cordilleran arc magmatism”. PhD thesis. Massachusetts Institute of Technology.
- (2010). “Managing the effects of accelerated glacial melting on volcanic collapse and debris flows: Planchon–Peteroa Volcano, Southern Andes”. *Global and Planetary Change* 74(2), pages 82–90. DOI: [10.1016/j.gloplacha.2010.08.003](https://doi.org/10.1016/j.gloplacha.2010.08.003).
- Tormey, D. R., F. A. Frey, and L. Lopez-Escobar (1995). “Geochemistry of the Active Azufre–Planchon–Peteroa Volcanic Complex, Chile (35 15’S): Evidence for Multiple Sources and Processes in a Cordilleran Arc Magmatic System”. *Journal of Petrology* 36(2), pages 265–298. DOI: [10.1093/ petrology/36.2.265](https://doi.org/10.1093/petrology/36.2.265).
- Tormey, D. R., R. Hickey-Vargas, F. A. Frey, and L. López-Escobar (1991). “Recent lavas from the Andean volcanic front (33 to 42 S); interpretations of along-arc compositional variations”. *Geological Society of America special paper* 265, pages 57–77.
- Tost, M., S. J. Cronin, and J. N. Procter (2014). “Transport and emplacement mechanisms of channelised long-runout debris avalanches, Ruapehu volcano, New Zealand”. *Bulletin of Volcanology* 76(12). DOI: [10.1007/s00445-014-0881-z](https://doi.org/10.1007/s00445-014-0881-z).
- Ui, T. (1983). “Volcanic dry avalanche deposits — Identification and comparison with nonvolcanic debris stream deposits”. *Journal of Volcanology and Geothermal Research* 18(1–4), pages 135–150. DOI: [10.1016/0377-0273\(83\)90006-9](https://doi.org/10.1016/0377-0273(83)90006-9).
- Valero-Garcés, B. L., B. Jenny, M. Rondanelli, A. Delgado-Huertas, S. J. Burns, H. Veit, and A. Moreno (2005). “Palaeohydrology of Laguna de Tagua Tagua (34° 30’ S) and moisture fluctuations in Central Chile for the last 46000yr”. *Journal of Quaternary Science* 20(7–8), pages 625–641. DOI: [10.1002/jqs.988](https://doi.org/10.1002/jqs.988).
- Valverde, V., P. A. Mothes, B. Beate, and J. Bernard (2021). “Enormous and far-reaching debris avalanche deposits from Sangay volcano (Ecuador): Multidisciplinary study and modeling the 30 ka sector collapse”. *Journal of Volcanology and Geothermal Research* 411, page 107172. DOI: [10.1016/j.jvolgeores.2021.107172](https://doi.org/10.1016/j.jvolgeores.2021.107172).
- Van Wyk de Vries, B., S. Self, P. Francis, and L. Keszthelyi (2001). “A gravitational spreading origin for the Socompa debris avalanche”. *Journal of Volcanology and Geothermal Research* 105(3), pages 225–247. DOI: [10.1016/s0377-0273\(00\)00252-3](https://doi.org/10.1016/s0377-0273(00)00252-3).
- Van Wyk de Vries, B., N. Kerle, and D. Petley (2000). “Sector collapse forming at Casita volcano, Nicaragua”. *Geology* 28(2), page 167. DOI: [10.1130/0091-7613\(2000\)28<167: scfacv>2.0.co;2](https://doi.org/10.1130/0091-7613(2000)28<167:scfacv>2.0.co;2).
- Vera, F., C. Perales, and R. G. Astorga (2021). “Evaluación geológica de puntos de encuentro transitorio en las comunas de Curacautín, Melipeuco, Cunco y Vilcún en caso de erupción del volcán Llaima”. *Servicio Nacional de Geología y Minería, Informe Técnico FIPVO*.
- Vigide, N., D. Yagupsky, H. Barcelona, M. Agosto, and A. Caselli (2020). “Structural analysis of the Planchón-Peteroa Volcanic Complex: Insights for the geothermal system”. *Journal of South American Earth Sciences* 104, page 102856. DOI: [10.1016/j.jsames.2020.102856](https://doi.org/10.1016/j.jsames.2020.102856).
- Voight, B. (1996). “The Management of Volcano Emergencies: Nevado del Ruiz”. *Monitoring and Mitigation of Volcano Hazards*. Edited by R. Scarpa and R. I. Tilling. Springer Berlin Heidelberg, pages 719–769. ISBN: 9783642800870. DOI: [10.1007/978-3-642-80087-0\\_22](https://doi.org/10.1007/978-3-642-80087-0_22).
- Völker, D., S. Kutterolf, and H. Wehrmann (2011). “Comparative mass balance of volcanic edifices at the southern volcanic zone of the Andes between 33°S and 46°S”. *Journal of Volcanology and Geothermal Research* 205(3–4), pages 114–129. DOI: [10.1016/j.jvolgeores.2011.03.011](https://doi.org/10.1016/j.jvolgeores.2011.03.011).
- Walker, G. P. L. (1993). “Basaltic-volcano systems”. *Geological Society, London, Special Publications* 76(1), pages 3–38. DOI: [10.1144/gsl.sp.1993.076.01.01](https://doi.org/10.1144/gsl.sp.1993.076.01.01).
- Walker, G. P. L. and D. H. Blake (1966). “The formation of a palagonite breccia mass beneath a valley glacier in Iceland”. *Quarterly Journal of the Geological Society* 122(1–4), pages 45–58. DOI: [10.1144/gsjgs.122.1.0045](https://doi.org/10.1144/gsjgs.122.1.0045).
- White, S. M., J. A. Crisp, and F. J. Spera (2006). “Long-term volumetric eruption rates and magma budgets”. *Geochemistry, Geophysics, Geosystems* 7(3). DOI: [10.1029/2005gc001002](https://doi.org/10.1029/2005gc001002).
- Yamagata, K. (1991). “Formation of lithic breccia and vent evolution during the 32 ka eruption of Shikotsu caldera, Japan”. *Geographical Reports of Tokyo Metropolitan University* 26, pages 227–240.
- Yoshida, H. (2013). “Decrease of size of hummocks with downstream distance in the rockslide-debris avalanche deposit at Iriga volcano, Philippines: similarities with Japanese avalanches”. *Landslides* 10(5), pages 665–672. DOI: [10.1007/s10346-013-0414-4](https://doi.org/10.1007/s10346-013-0414-4).